Supporting Information

for

Unravelling Solid-state Microstructure from Conjugated Oligomers to Polymers

Yu-Chun Xu, Yang-Yang Zhou, Li Ding, Yi-Zhen Zhang, Ze-Fan Yao, Yu Shao, Yi Liu, Jie-Yu Wang, Wen-Bin Zhang*, and Jian Pei*

Beijing National Laboratory for Molecular Sciences (BNLMS), Key Laboratory of Polymer Chemistry and Physics of Ministry of Education, Center for Soft Matter Science and Engineering, College of Chemistry and Molecular Engineering, Peking University, Beijing 100871, P. R. China

Table of contents

1. General procedures and experimental details.

All commercially available chemicals were used without further purification unless otherwise noted. All air and water sensitive reactions were performed under N_2 atmosphere. ^1H and ^{13}C NMR spectra of small molecules and oligomers were recorded on Bruker-400 MHz (AVANCE III), Bruker-500 MHz (AVANCE III) and Bruker-600 MHz. All chemical shifts were reported in parts per million (ppm). Molecular weight of all polymers was determined by gel permeation chromatography (GPC) performed on Polymer Laboratories PL-GPC220 at 150 °C using 1,2,4-tricholorobenzene (TCB) as eluent. Differential scanning calorimetry (DSC) analyses were performed on a METTLER TOLEDO Instrument DSC822 calorimeter. Absorption spectra were recorded on PerkinElmer Lambda 750 UV-*vis* spectrometer. Varied-temperature absorption spectra were recorded on Shimadzu UV3600Plus spectrometer. Atomic force microscopies (AFM) were performed with Cypher S microscope (Asylum Research, Oxford Instruments) at tapping mode under ambient conditions using silicon cantilever (AC240TS-R3) with a resonant frequency around 70 kHz. Grazing incidence wide-angle X-ray scattering (GIWAXS) and wide-angle X-ray scattering (WAXS) were performed in vacuum on a Ganesha SAXSLAB instrument using the Cu Kα irradiation (wavelength of 1.54 Å) with thin-film and powder, respectively. The critical angle α_c is given by

$$\alpha_c = \lambda \sqrt{\frac{r_e \rho}{\pi}} \qquad (1)$$

Where r_e is the Thomson scattering length of the electron (=2.817 × 10^{-5} $Å^{-1}$) and ρ is the electron density of the materials. For conjugated polymers ρ ≈ 0.4 $Å^{-3}$ and hence critical angle of conjugated polymers is ~0.17°.[1] The angle of incidence for GIWAXS is 0.20°.

Thin films devices fabrications and characterization.

BG/TC FET devices were fabricated using n^{++}-Si/SiO_2 (300 nm) substrates. The substrates were subjected to cleaning using ultrasonication in acetone, detergent, deionized water, and isopropyl alcohol. The cleaned substrates were dried over a nitrogen airflow. All the above processes were performed under ambient conditions. The substrates were modified with octadecyltrimethoxysilane (OTS) to form a SAM monolayer. Thin films of the oligomers and polymer were deposited on the treated substrates by spin coating using a solution (10 mg/mL for oligomers *n*IID, n = 3, 4, and 5 mg/mL for oligomers *n*IID, n = 6 and 8 and polymer PIID), optionally followed by thermal annealing at 120 °C for 3IID-318 and 4IID-318, 180 °C for other oligomers *n*IID and polymers PIIDs under nitrogen. After polymer thin film deposition, 40 nm thick gold were deposited as source and drain contacts using a shadow mask. The organic field effect transistors (OFET devices) had a channel length (*L*) of 1200 μm and a channel width (*W*) of 30 μm. The evaluations of the FETs were carried out under ambient conditions (22 °C, R_H = 0-60%) on a probe stage using a Keithley 4200 SCS as parameter analyzer. The carrier mobility (μ) was calculated from the data in the saturated regime according to the equation I_{SD}

= $(W/2L)C_i\mu(V_G\text{-}V_T)^2$, where I_{SD} is the drain current in the saturated regime. C_i (C_i = 11 nF cm^{-2}) is the capacitance per unit area of the gate dielectric layer, and V_G and V_T are the gate voltage and threshold voltages. V_G-V_T of the device was determined from the relationship between the square root of I_{SD} and V_G at the saturated regime.

Molecular modelling.

The molecular geometry of oligomers was optimized at the B3LYP/6-31g(d) level of theory.[2,3] The optimized oligomers molecules were used to construct the initial crystal structure with periodic boundary conditions. Alkyl chains were carefully set with fully extended. The cell parameters were initialized according to WAXS data. The crystal structure was optimized with COMPASSIII force field.[4] The relaxed structure was subjected to a quenched dynamics simulation (NPT, 1000 ps, $P = 1 \times 10^5$ Pa, T = 300 K, quench frequency = 10 ps).[5] The unit cell was used to construct the supercell to simulate the crystalline phase. 3 × 3 × 3 supercell of oligomers (n = 3 and 4), 3 × 3 × 2 supercell of oligomers (n = 6 and 8) and 3 × 3 × 12 supercell of polymers were constructed. Two consecutive molecular dynamics calculations have been performed on each supercell: (i) the first one for thermalization (NPT, $P = 1 \times 10^5$ Pa, T = 298 K, 200 ps); (ii) and then for data analysis (NPT, $P = 1 \times 10^5$ pa, T = 298 K, 200 ps, snapshots saved every 1 ps). All molecular simulations were performed with Materials Studio package. COMPASSIII force field, Velocity Scale themostat, Pamnello barostat. The following protocol is to simulate an amorphous phase of polymer: (i) 24 dodecamer have been put randomly in a large unit cell and keep the density of about 0.02 g/cm^3. 200 ps molecular dynamics (NVT, T = 1000 K) have been run to obtain random distribution of the polymers; 4 successive 200 ps molecular dynamics (NPT, $P = 1 \times 10^5$ Pa) were then performed at decreasing temperature (1000, 500, 350 and 298 K, respectively); A 200 ps molecular dynamics (NPT, $P = 1 \times 10^5$ Pa, T = 298 K) was performed and snapshots saved every 1ps for further analysis.[6] The simulation of GIWAXS pattern was performed with the polymer crystal structure using SimDiffraction codes.[7]

2. Synthesis and characterization

All commercially available chemicals were used without further purification unless otherwise noted. The monomers, IID-310 and IID-318, were synthesized following our reported procedures.[8,9]

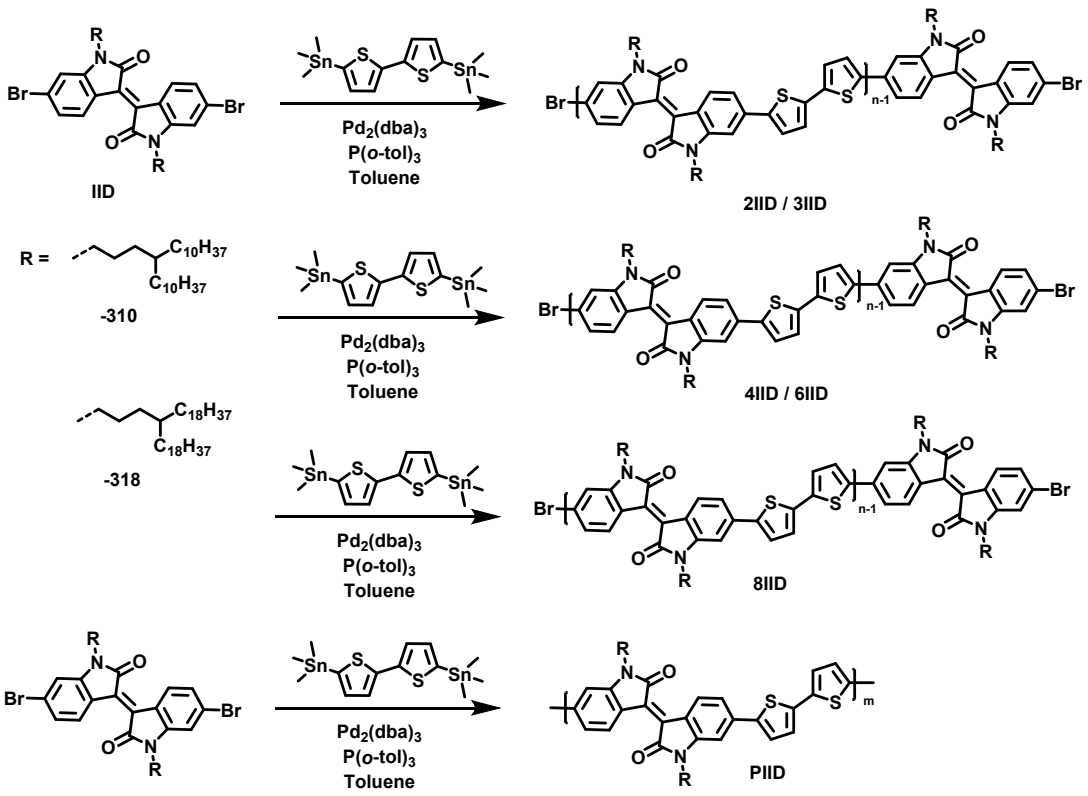

Scheme S1. Synthetic approach to *n*IID-310s, *n*IID-318s and polymer PIID-318.

2IID-310 and ***3IID-310.*** To a Schlenk tube IID-310 (500 mg, 0.45 mmol), 2,5-bis(trimethylstannyl)thiophene (31.96 mg, 0.065mmol), $Pd_2(dba)_3$ (2.34 mg, 4 mol%), P(*o*-tol)$_3$ (3.12 mg, 16 mol%), and toluene (60 mL) were added. After freeze-pump-thaw cycles, the mixture was stirred at 100 °C for 24 h. The mixture was allowed to room temperature. After the solvent was removed under reduced pressure, the residue was purified by column chromatography on silica gel with eluent (PE:DCM = 4:1) to give 2IID-310 (96 mg, yield 58%) as purple solids and 3IID-310 (43 mg, yield 26%) as blue solids.

2IID-310: ^{1}H NMR (400 MHz, $C_2D_2Cl_4$, ppm): δ 9.21-9.19 (d, *J* = 8.4 Hz, 2H), 9.10-9.08 (d, *J* = 8.6 Hz, 2H), 7.40-7.39 (d, *J* = 3.9 Hz, 2H), 7.26-7.24 (m, 4H), 7.15-7.12 (dd, *J* = 7.3, 1.8Hz, 2H), 6.95 (m, 4H), 3.81-3.77 (m, 4H), 3.73-3.70 (m, 4H), 1.73-1.66 (m, 8H), 1.38-1.22 (m,156H), 0.88-0.83 (m, 24H). ^{13}C NMR (101 MHz, $C_2D_2Cl_4$, ppm): 167.0, 166.7, 144.6, 144.5, 142.0, 136.9, 136.6, 132.0, 130.3, 130.0, 130.0, 129.7, 129.7, 129.7, 125.3, 124.0, 120.1, 120.0, 118.1, 110.3, 103.4, 39.7, 36.2, 36.1, 32.6, 31.0, 30.0, 29.3, 29.3, 28.9, 28.9, 28.8, 28.5, 25.8, 23.6, 21.8, 13.4. MALDI-HRMS calcd. for $C_{136}H_{213}Br_2N_4O_4S_2$ ($[M + H]^+$): 2188.4390; Found: 2188.4345.

3IID-310: ^{1}H NMR (500 MHz, $C_2D_2Cl_4$, 90 °C, ppm): δ 9.30-9.28 (m, 4H), 9.17-9.15 (d, *J* = 8.4 Hz, 2H), 7.43-7.42 (m, 4H), 7.36-7.34 (m, 4H), 7.31-7.30 (m, 4H), 6.24-7.22 (dd, *J* = 8.7, 1.8 Hz, 2H), 7.04-7.03 (m, 4H), 6.99-6.98 (d, *J* = 1.8 Hz, 2H), 3.90-3.86 (m, 8H), 3.73-3.70 (t, *J* = 7.0 Hz, 4H), 1.86-1.75 (m, 12H), 1.48-1.31 (m, 234H) 0.95-0.91 (m, 36H). ^{13}C NMR (101 MHz, $CDCl_3$, ppm): δ 168.0, 167.9, 167.6, 162.5, 153.8, 149.3, 145.3, 145.2, 144.8, 142.9, 142.5, 137.9, 137.4, 137.1, 136.4, 132.6, 131.0, 130.7, 125.9, 124.6, 121.1, 120.8, 120.6, 110.9, 103.9, 103.5, 97.1, 37.2, 33.6, 32.0, 31.0, 30.3, 30.2, 29.8, 29.8, 29.7, 29.4, 26.7, 22.7, 14.2. MALDI-HRMS calcd. for $C_{208}H_{321}Br_2N_6O_6S_4$ ($[M + H]^+$): 3285.2242; Found: 3285.2244.

4IID-310 and ***6IID-310.*** To a Schlenk tube 2IID-310 (142 mg, 0.064 mmol), 2,5-bis(trimethylstannyl)thiophene (7.98 mg, 0.016 mmol), $Pd_2(dba)_3$ (0.60 mg, 4 mol%), P(*o*-tol)$_3$ (0.79 mg, 16 mol%), and toluene (30 mL) were added. After freeze-pump-thaw cycles, the mixture was stirred at 100 °C for 24 h. The mixture was allowed to room temperature. After the solvent was removed under reduced pressure, the residue was purified by column chromatography on silica gel with eluent (PE:CF = 2:1) to give 4IID-310 (22 mg, yield 32%) as black solids and 6IID-310 (13 mg, 12%) as black solids.

4IID-310: ^{1}H NMR (500 MHz, $C_2D_2Cl_4$, 90 °C, ppm): δ 9.24-9.23 (m, 6H), 9.13-9.11 (d, *J* = 8.6 Hz, 2H), 7.37-7.36 (m, 6H), 7.30-7.27 (m, 6H), 7.24-7.23 (m, 6H), 7.19-7.18 (dd, *J* = 8.6, 1.6 Hz, 2H), 6.96 (m, 6H), 6.94 (d, *J* = 1.6Hz, 2H), 3.87-3.74 (m, 16H), 1.82-1.74 (m, 16H), 1.43-1.29 (m, 312H), 0.93-0.89 (m, 48H). ^{13}C NMR (126 Hz, $C_2D_2Cl_4$, 90 °C, ppm): δ 168.0, 167.5, 145.8, 145.3, 143.1, 142.8, 138.3, 137.6, 137.0, 133.6, 132.9, 131.7, 131.5, 131.1, 131.0, 130.5, 129.9, 128.9, 126.0, 125.0, 124.6, 123.2, 121.5, 120.7, 120.3, 119.2, 118.8, 112.1, 111.0, 104.1, 103.9, 40.5, 37.8, 34.2, 31.7, 31.2, 30.0, 29.5, 29.1, 26.7, 24.7, 22.4, 13.8. MALDI-HRMS calcd. for $C_{280}H_{429}Br_2N_8O_8S_6$ ($[M + H]^+$): 4382.0094; Found: 4381.9937.

6IID-310: ^{1}H NMR (500 MHz, $C_2D_2Cl_4$, 90 °C, ppm): δ 9.24-9.09 (m, 12H), 7.40-6.84 (m, 44H), 3.86-3.77 (m, 24H), 1.81-1.75, 24H), 1.31 (m, 468H), 0.93-0.91 (m, 72H). Because of the strong intermolecular interaction, it is difficult to obtain the ^{13}C NMR with high resolution. MALDI-HRMS calcd. for $C_{424}H_{645}Br_2N_{12}O_{12}S_{10}$ ($[M + H]^+$): 6575.5798; Found: 6575.5775.

8IID-310: To a Schlenk tube 4IID-310 (200 mg, 0.046mmol), 2,5-bis(trimethylstannyl)thiophene (3.74 mg, 0.007 mmol), $Pd_2(dba)_3$ (0.26 mg, 4 mol%), P(*o*-tol)$_3$ (0.34 mg, 16 mol%), and toluene (20 mL) were added. After freeze-pump-thaw cycles, the mixture was stirred at 100 °C for 24 h. The mixture was allowed to room temperature. After the solvent was removed under reduced pressure, the residue was purified by preparative GPC with $CHCl_3$ as the eluent to give 8IID-310 as black solids (36 mg, yield 54%). ^{1}H NMR (500 MHz, $C_2D_2Cl_4$, 90 °C, ppm): *δ* 9.13-9.10 (m, 16H), 7.21-6.71 (m, 60H), 3.83-3.73 (m, 32H), 1.82-1.73 (m, 32H), 1.50-1.31 (m, 624H), 0.94-0.90 (m, 98H). MALDI-HRMS calcd. for $C_{568}H_{861}Br_2N_{16}O_{16}S_{14}$ ($[M + H]^+$): 8769.1503; Found: 8769.1871.

PIID-310: To a Schlenk tube IID-318 (80 mg, 0.073 mmol), 2,5-bis(trimethylstannyl)thiophene (36 mg, 0.073 mmol), $Pd_2(dba)_3$ (2.67 mg, 4 mol%), P(*o*-tol)$_3$ (3.68 mg, 16 mol%), and toluene (10 mL) were added. After where freeze-pump-thaw cycles, the mixture was stirred at 110 °C for 30 min. *N*,*N*'-Diethylphenylazothioformamide (20 mg) was then added and then the mixture was stirred for 30 min to remove any residual catalyst before being precipitated into methanol (250 mL). The precipitate was filtered through a nylon filter and purified via Soxhlet extraction for 4 h with acetone, 4 h with hexane, 24 h with chloroform, and finally was collected with chlorobenzene. The chlorobenzene solution was then concentrated by evaporation and precipitated into methanol (200 mL) and filtered off as blue dark solids (76 mg, yield 92%).

2IID-318 and ***3IID-318.*** To a Schlenk tube IID-318 (600 mg, 0.39 mmol), 2,5-bis(trimethylstannyl)thiophene (47.9 mg, 0.065mmol), $Pd_2(dba)_3$ (3.56 mg, 4 mol%), P(*o*-tol)$_3$ (4.74 mg, 16 mol%), and toluene (60 mL) were added. After freeze-pump-thaw cycles, the mixture was stirred at 100 °C for 24 h. The mixture was allowed to room temperature. After the solvent was removed under reduced pressure, the residue was purified by column chromatography on silica gel with eluent (PE:DCM = 4:1) to give 2IID-318 (64 mg, yield 32%) as purple solids and 3IID-318 (76 mg, yield 17%) as blue solids.

2IID-318: ^{1}H NMR (400 MHz, $C_2D_2Cl_4$, ppm): δ 9.17-9.16 (d, J = 8.4 Hz, 2H), 9.05-9.03 (d, J = 8.6 Hz, 2H), 7.36-7.35 (d, J = 3.9 Hz, 2H), 7.28-7.19 (m, 4H), 7.16-7.14 (d, J = 8.7 Hz, 2H), 6.90 (m, 4H), 3.78-3.72 (m, 8H), 1.82-1.52 (m, 8H), 1.23 (m, 284H), 0.97-0.76 (m, 24H). ^{13}C NMR (151 MHz, $C_2D_2Cl_4$, ppm): δ 167.8, 167.5, 145.4, 145.3, 142.8, 137.7, 137.4, 132.8, 131.1, 130.8, 130.5, 126.1, 125.4, 125.1, 124.8, 120.9, 120.5, 118.9, 111.0, 104.2, 74.1, 74.0, 73.8, 73.6, 40.4, 40.3, 37.0, 36.9, 33.4, 31.9, 30.7, 30.6, 30.1, 30.06, 29.69, 29.67, 29.61, 29.3, 26.62, 26.59, 24.4, 22.7, 14.2. MALDI-HRMS calcd. for $C_{200}H_{341}Br_2N_4O_4S_2$ ($[M + H]^+$): 3085.4406; Found: 3085.4378.

3IID-318: ^{1}H NMR (400 MHz, $C_2D_2Cl_4$, ppm): δ 9.05-9.04 (m, 4H), 8.98-8.96 (d, J = 4.8 Hz, 2H), 7.23-7.21 (m, 4H), 7.09-7.04 (m, 10H), 6.78-6.70 (m, 6H), 3.72-3.66 (m, 12H), 1.67-1.62 (m, 12H), 1.35-1.18 (m, 426H), 0.85-0.81 (m, 36H). ^{13}C NMR (151 MHz, $C_2D_2Cl_4$, ppm): δ 167.7, 167.4, 145.2, 142.8, 142.5, 137.8, 137.4, 137.2, 136. 6, 131.3, 131.2, 130.1, 125.9, 124.8, 121.0, 120.7, 120.4, 118.4, 110.9, 103.8, 103.3, 74.1, 74.0, 73.8, 73.6, 40.3, 37.0, 36.98, 36.95, 33.47, 33.43, 31.9, 30.8, 30.16, 30.13, 30.09, 29.74, 29.68, 29.62, 29.3, 26.7, 26.63, 26.60, 24.4, 22.7, 14.16, 14.15. MALDI-HRMS calcd. for $C_{304}H_{513}Br_2N_6O_6S_4$ ($[M + H]^+$): 4630.7266; Found: 4630.7124.

4IID-318 and ***6IID-318.*** To a Schlenk tube 2IID-318 (292 mg, 0.095 mmol), 2,5-bis(trimethylstannyl)thiophene (9.32 mg, 0.019 mmol), $Pd_2(dba)_3$ (0.70 mg, 4 mol%), P(*o*-tol)$_3$ (0.93 mg, 16 mol%), and toluene (30 mL) were added. After freeze-pump-thaw cycles, the mixture was stirred at 100 °C for 24 h. The mixture was allowed to room temperature. After the solvent was removed under reduced pressure, the residue was purified by column chromatography on silica gel with eluent (PE:CF

= 2:1) to give 4IID-318 (46 mg, yield 39%) as black solids and 6IID-318 (17 mg, 10%) as black solids.

4IID-318: ^{1}H NMR (500 MHz, $C_2D_2Cl_4$, 90 °C, ppm): δ 9.30-9.29 (m, 6H), 9.16-9.14 (d, J = 6.5 Hz, 2H), 7.41-7.40 (m, 6H), 7.35-7.32 (m, 6H), 7.29-7.28 (m, 6H), 7.22-7.20 (dd, J = 8.5, 1.8 Hz, 2H), 7.02-7.01 (m, 6H), 6.97 (d, J = 1.2 Hz, 2H), 3.89-3.84 (m, 12H) 3.79-3.16 (t, J = 6.5 Hz, 4H), 1.83-1.49 (m, 16H) 1.44-1.30 (m, 568H), 0.94-0.90 (m, 48H). ^{13}C NMR (151 MHz, $CDCl_3$, ppm): δ 168.0, 168.0, 167.7, 167.4, 145.3, 145.2, 144.8, 142.9, 142.7, 142.5, 137.9, 137.6, 137.4, 137.2, 136.3, 132.6, 131.0, 130.7, 125.9, 124.6, 121.2, 120.8, 120.7, 118.3, 118.0, 110.9, 103.6, 77.3, 77.1, 76.9, 40.5, 37.3, 37.3, 37.2, 33.7, 33.6, 32.0, 31.2, 31.1, 30.3, 30.3, 30.3, 29.9, 29.9, 29.8, 29.8, 29.8, 29.4, 28.4, 27.1, 26.8, 26.8, 24.9, 24.8, 22.8, 14.2. MALDI-HRMS calcd. for $C_{408}H_{685}Br_2N_8O_8S_6$ ([M + H]$^+$): 6176.0126; Found: 6175.9826.

6IID-318: ^{1}H NMR (500 MHz, $C_2D_2Cl_4$, 90 °C, ppm): δ 9.27-9.22 (m, 10H), 9.15-9.13 (d, J = 6.4 Hz, 2H), 7.38-7.17 (m, 32H), 6.97-6.90 (m, 12H), 3.86-3.77 (m, 24H), 1.83-1.74 (m, 24H), 1.48-1.31 (m, 852H), 0.94-0.88 (m, 72H). Because of the strong intermolecular interaction, it is difficult to obtain the ^{13}C NMR with high resolution. MALDI-HRMS calcd. for $C_{616}H_{1029}Br_2N_{12}O_{12}S_{10}$ ([M + H]$^+$): 9265.5847; Found: 9266.5119.

8IID-318: To a Schlenk tube 4IID-318 (400 mg, 0.065 mmol), 2,5-bis(trimethylstannyl)thiophene (5.32 mg, 0.011 mmol), $Pd_2(dba)_3$ (0.39 mg, 4 mol%), P(*o*-tol)$_3$ (0.53 mg, 16 mol%), and toluene (40 mL) were added. After freeze-pump-thaw cycles, the mixture was stirred at 100 °C for 24 h. The mixture was allowed to room temperature. After the solvent was removed under reduced pressure, the residue was purified by preparative GPC with CHCl3 as the eluent to give 8IID-318 as black solids (61 mg, yield 46%). ^{1}H NMR (500 MHz, $C_2D_2Cl_4$, 90 °C, ppm): δ 9.16-9.13 (m, 16H), 7.26-6.77 (m, 60H), 3.81-3.72 (m, 32H), 1.79-1.70 (m, 32H), 1.45-1.27 (m, 1336H), 0.90-0.87 (m, 96H). MALDI-MS calcd. for $C_{824}H_{1372}Br_2N_{16}O_{16}S_{14}$ ([M + H$^+$]): 12369.79; Found: 12370.09.

PIID-318: To a Schlenk tube IID-318 (100 mg, 0.064 mmol), 2,5-bis(trimethylstannyl)thiophene (31.90 mg, 0.064 mmol), $Pd_2(dba)_3$ (2.37 mg, 4 mol%), P(*o*-tol)$_3$ (3.15 mg, 16 mol%), and toluene (10 mL) were added. After where freeze-pump-thaw cycles, the mixture was stirred at 110 °C for 1 h. *N*,*N*'-Diethylphenylazothioformamide (20 mg) was then added and then the mixture was stirred for 30 min to remove any residual catalyst before being precipitated into methanol (250 mL). The precipitate was filtered through a nylon filter and purified via Soxhlet extraction for 4 h with acetone, 4 h with hexane, 24 h with chloroform, and finally was collected with chlorobenzene. The chlorobenzene solution was then concentrated by evaporation and precipitated into methanol (200 mL) and filtered off as blue dark solids (40 mg, yield 40%).

Table S1. The molecular weights of PIID-310 and PIID-318 (1,2,4-tricholorobenzene as eluent at 150 °C).

Polymer	M_n (Da)	M_w (Da)	$Đ_M$
PIID-310	28639	65246	2.28
PIID-318	80570	192746	2.39

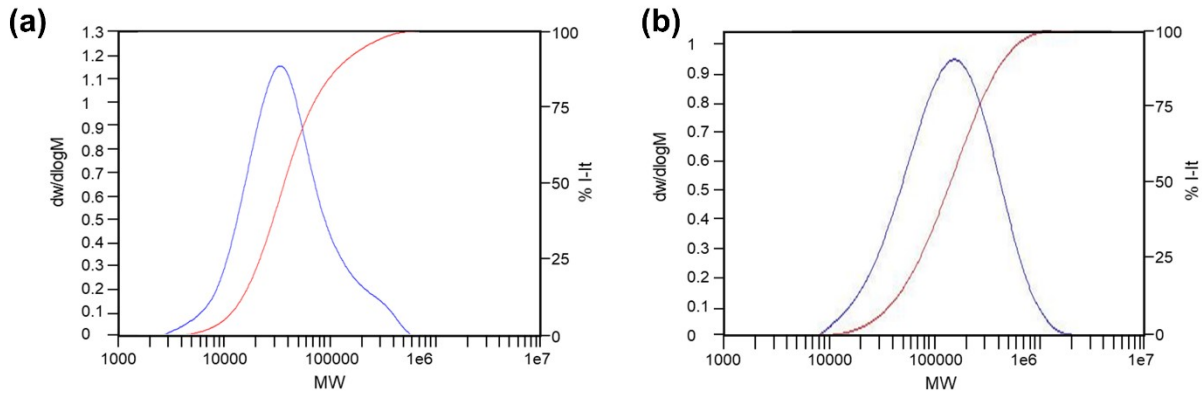

Figure S1. Molecular weights and dispersity of the polymers: (a) PIID-310 and (b) PIID-318. The molecular weight distributions of two polymers, PIID-310 and PIID-318, were measured by high-temperature gel permeation chromatography (GPC) at 150 °C.

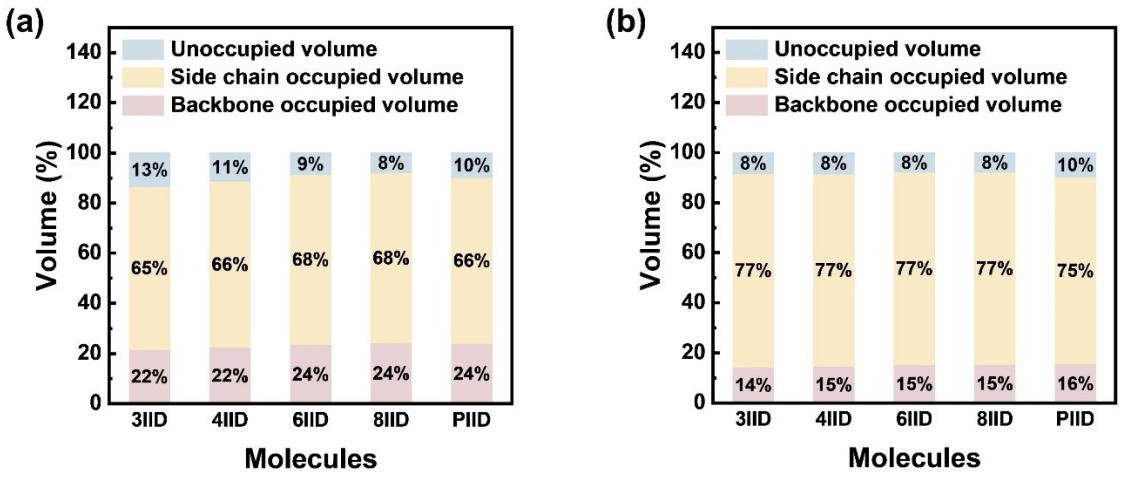

Figure S2. Atom occupied volume of side chain and backbone of oligomers calculated from molecular dynamics simulation: (a) *n*IID-310s and (b) *n*IID-318s.

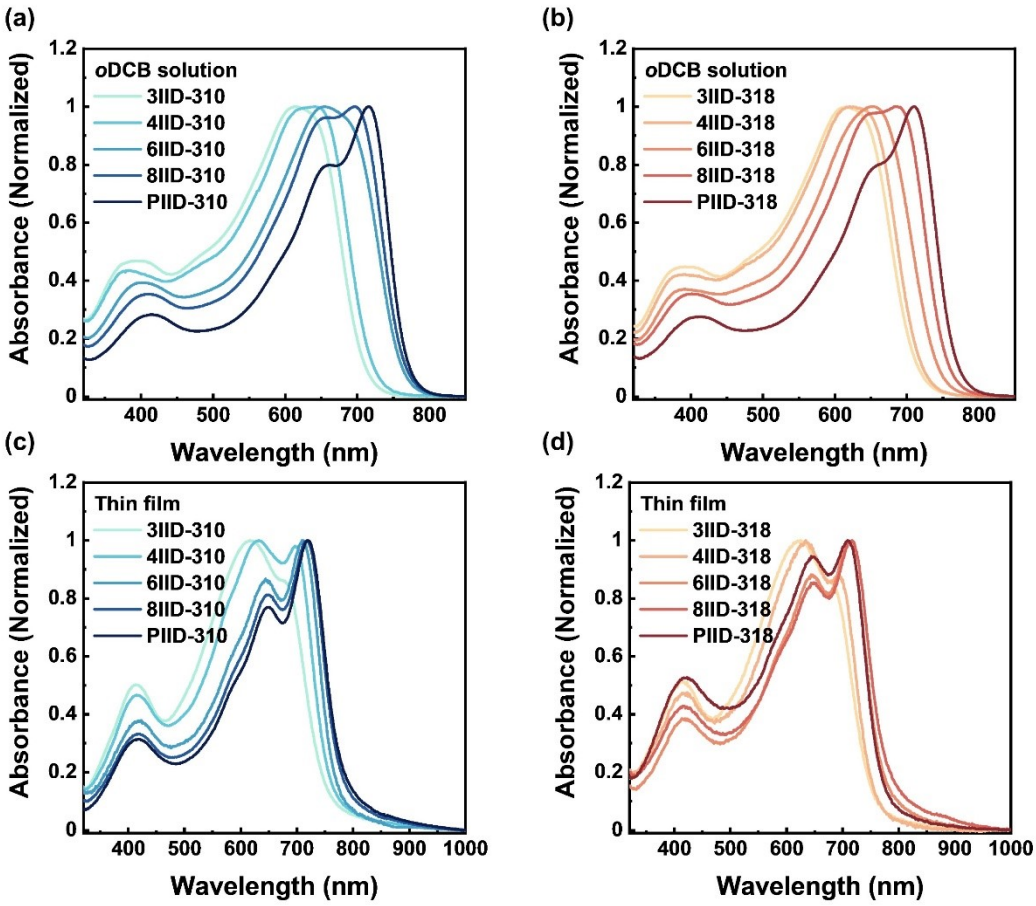

Figure S3. UV-*vis* absorption spectra of oligomers and polymer of *n*IID-310s and *n*IID-318s: (a) 0.02 g/L of *n*IID-310s *o*DCB solution at room temperature. (b) 0.02 g/L of *n*IID-310s *o*DCB solution at room temperature. (c) Thin film of *n*IID-310s. (d) Thin film of *n*IID-318s.

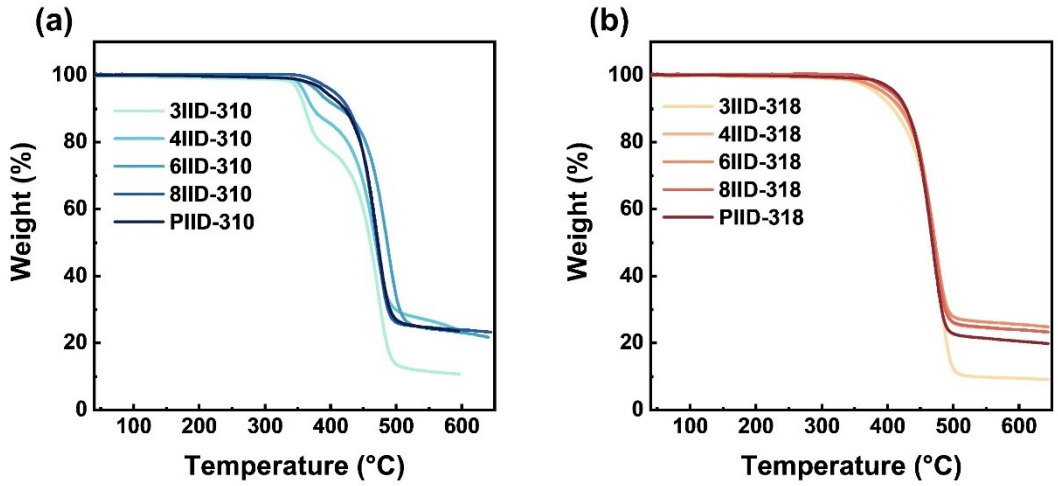

Figure S4. Thermogravimetric analysis of *n*IID-310s and *n*IID-318s.

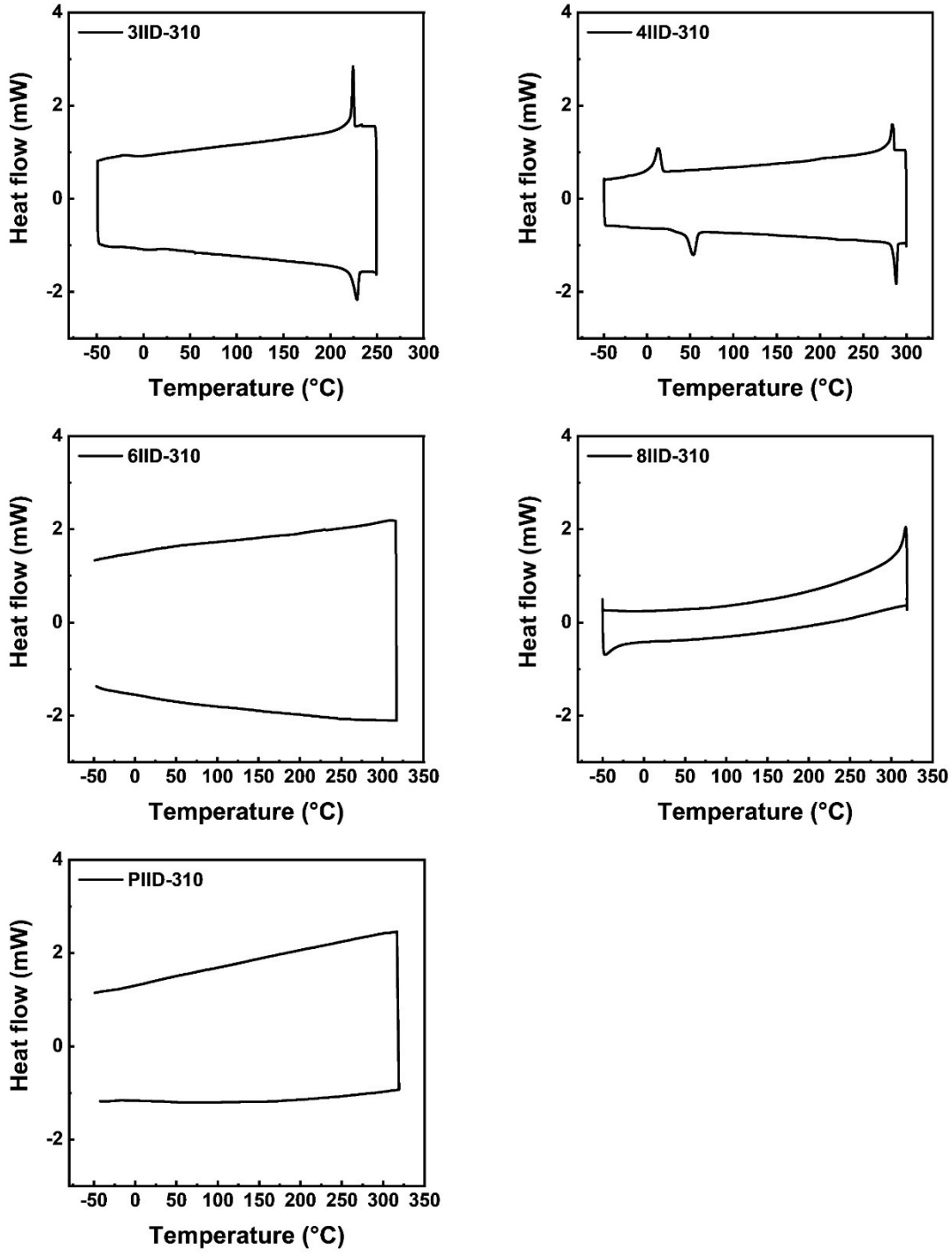

Figure S5. DSC thermogram of the second cycle of oligomers *n*IID-310s and polymer PIID-310.

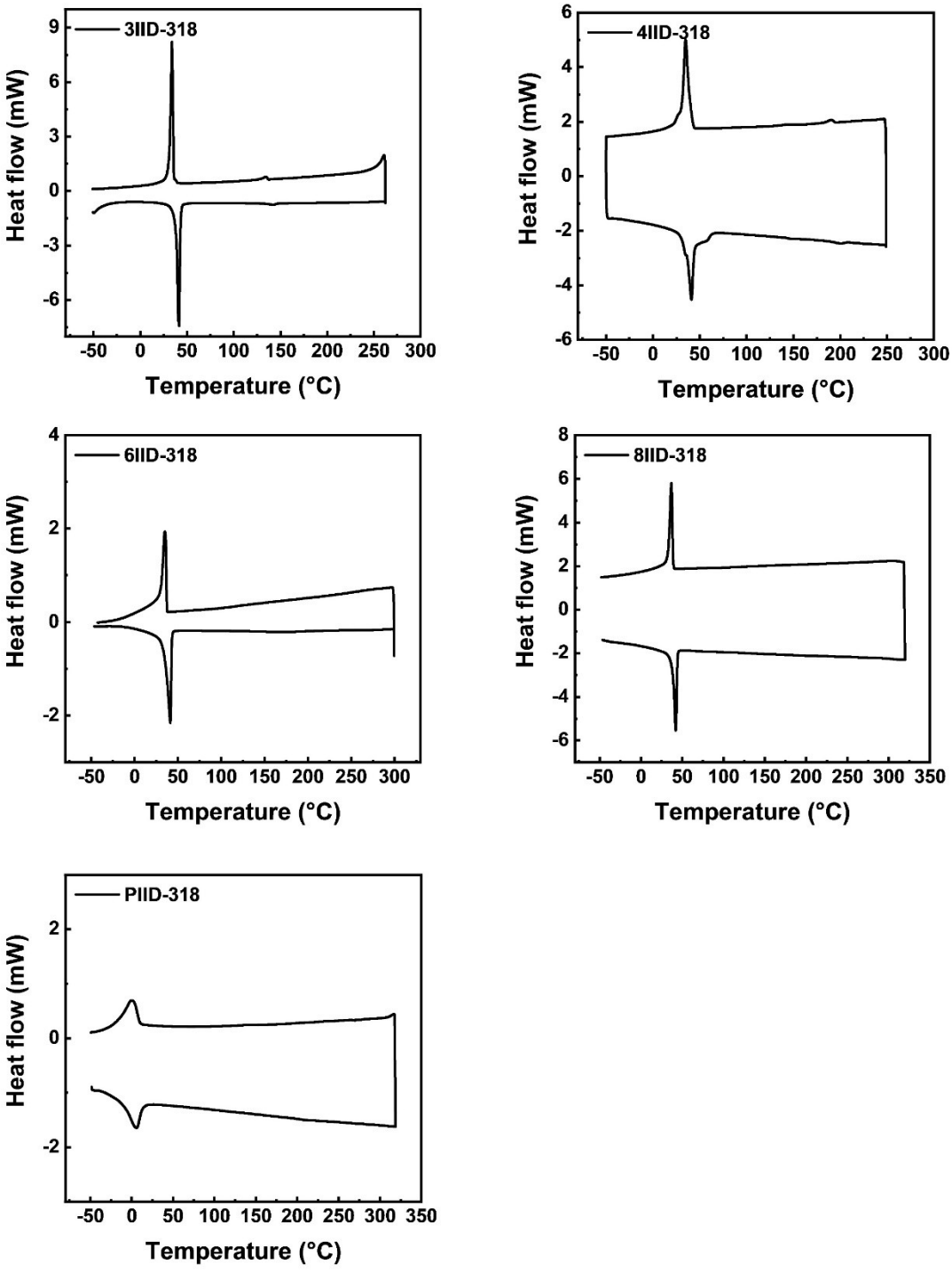

Figure S6. DSC thermogram of the second cycle of oligomers *n*IID-318s and polymer PIID-318.

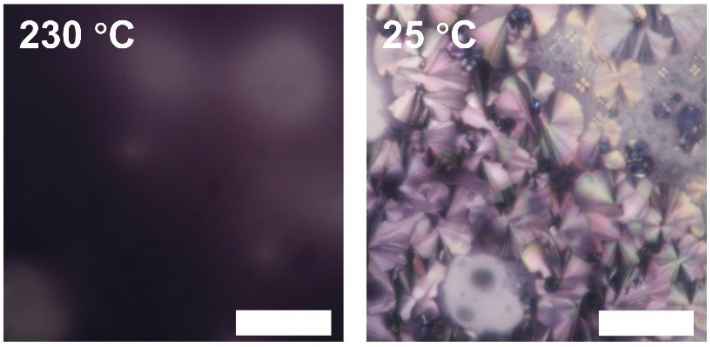

Figure S7. Optical textures observed under POM of 3IID-310 (scale bar, 50 μm).

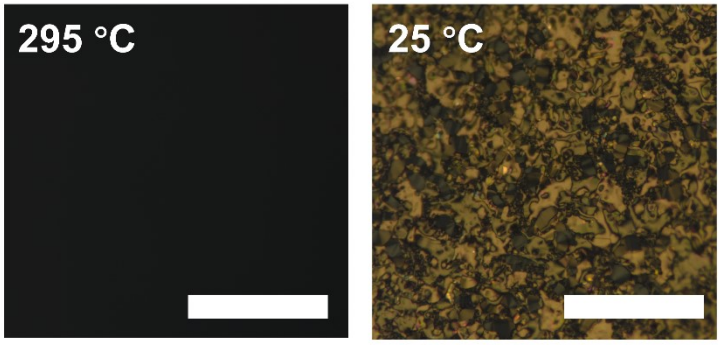

Figure S8. Optical textures observed under POM of 4IID-310 (scale bar, 50 μm).

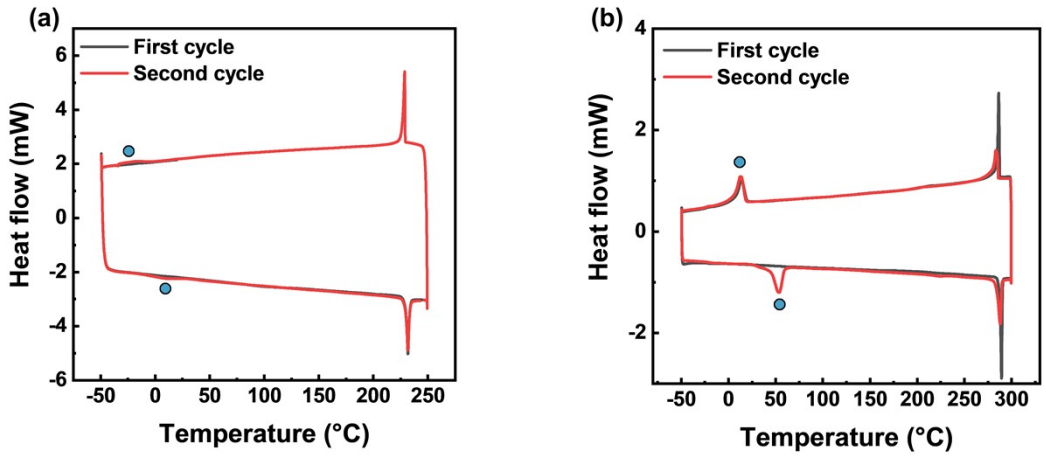

Figure S9. DSC thermogram of (a) 3IID-310. (b) 4IID-310.

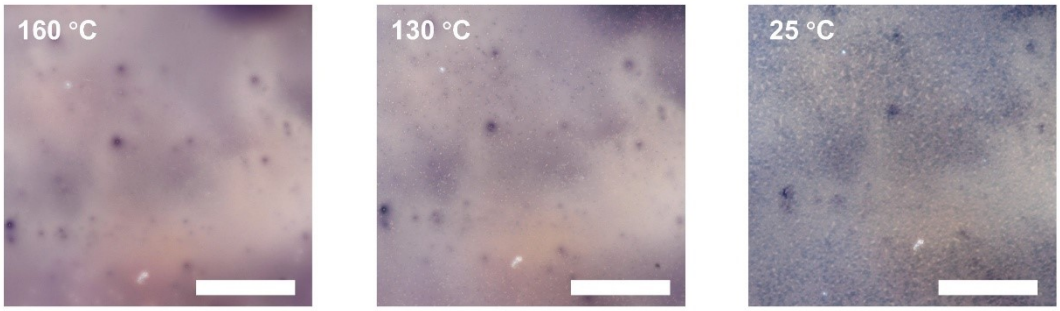

Figure S10. Optical textures observed under POM of 3IID-318 (scale bar, 50 μm).

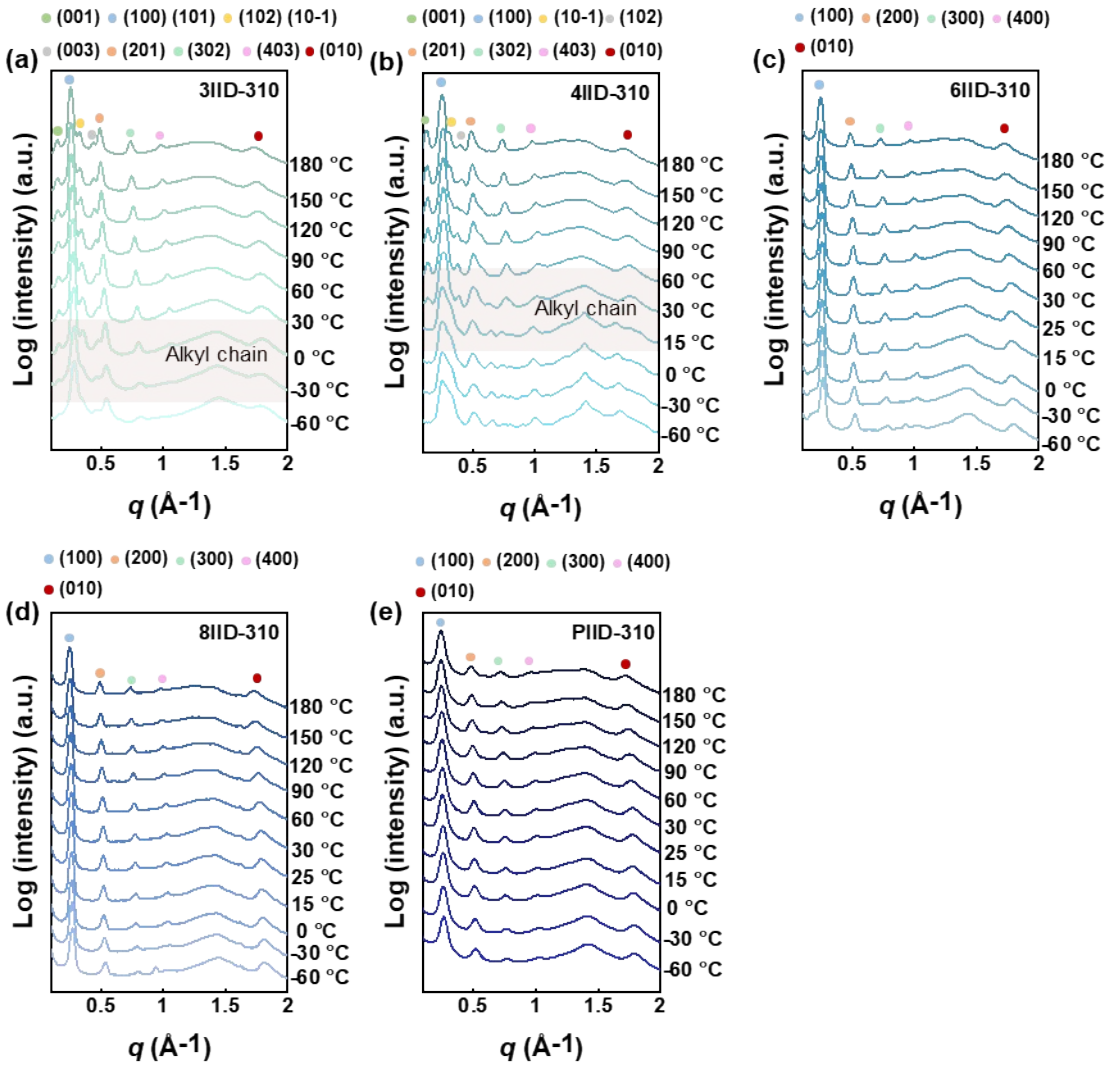

Figure S11. Temperature-dependent (cooling process) powder wide-angle X-ray scattering (WAXS) of *n*IID-310s. Upon decreasing the temperature to the crystallization point, 3IID-310 and 4IID-310 showed a weakening of lamellar packing and π–π packing along with an increasing of alkyl chain packing (brown box).

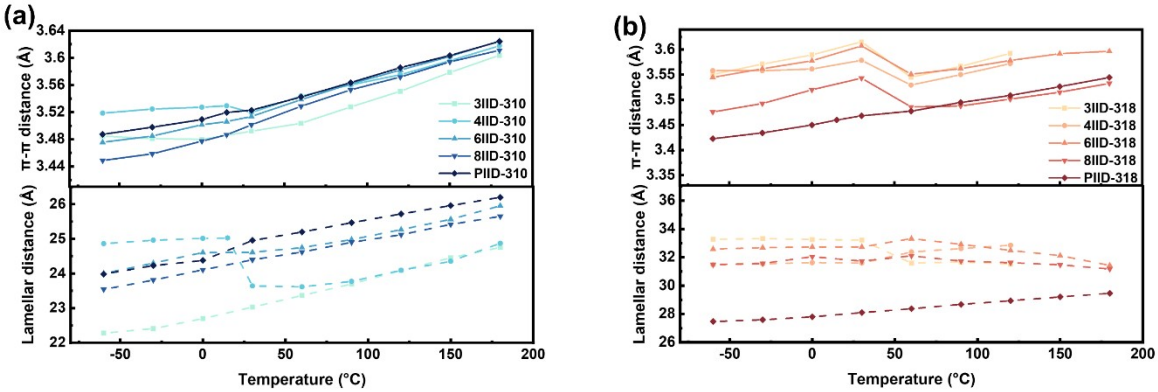

Figure S12. (a) Curves of lamellar distance and π–π distance versus temperature for *n*IID-310s. (b) Curves of lamellar distance and π–π distance versus temperature for *n*IID-318s.

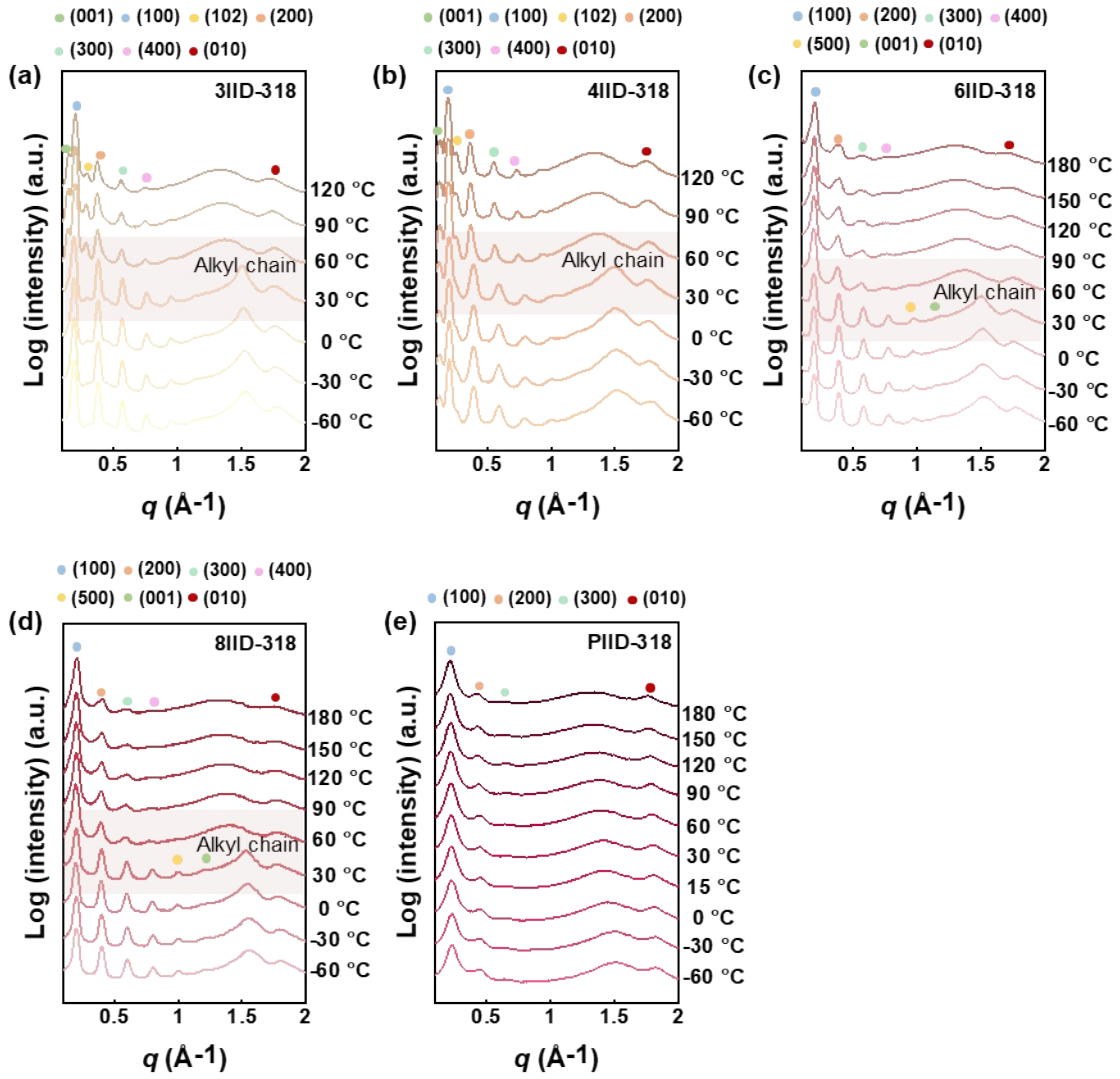

Figure S13. Temperature-dependent (cooling process) powder wide-angle X-ray scattering (WAXS) of *n*IID-318s. When the temperature was lowered to the crystallization temperature of the alkyl chains, a significant diffraction signal was observed in the alkyl chain region, along with a decrease in the half-peak widths of the lamellar packing and π–π packing diffractions. The packing of alkyl chains facilitates the stabilization of the backbone packing. However, the backbone π–π distance increases due to the mismatch between the alkyl chain packing and the backbone packing (brown box).

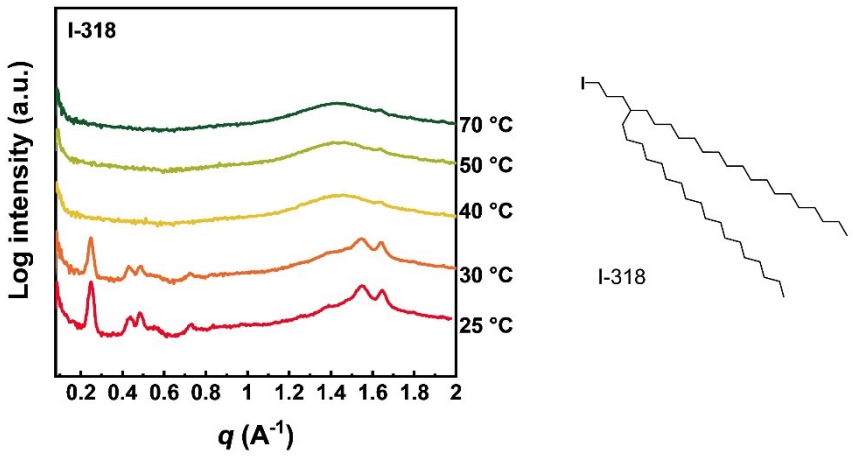

Figure S14. Temperature-dependent (cooling process) powder small-angle X-ray scattering (WAXS) of 19-(3-iodopropyl)heptatriacontane (I-318).

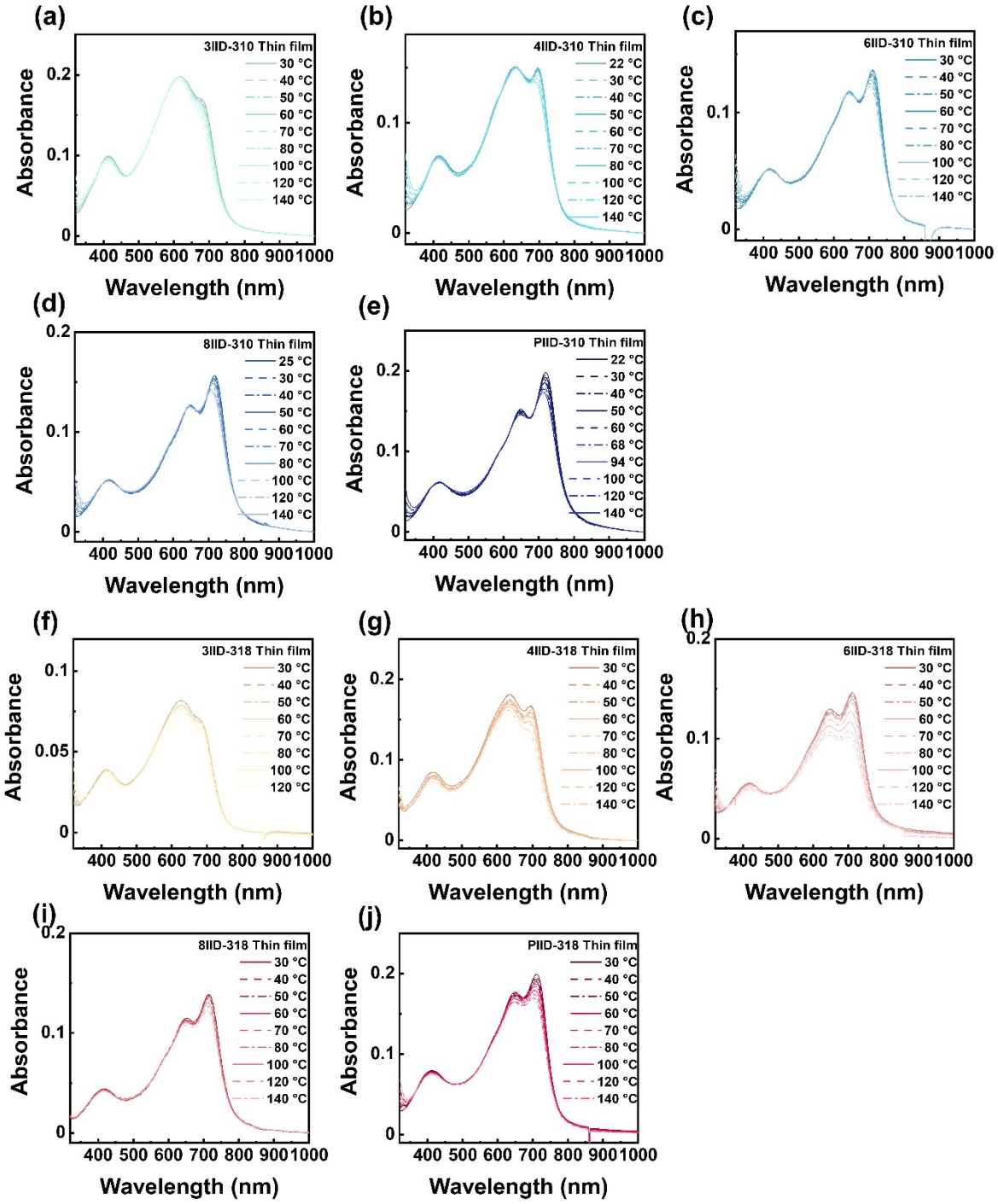

Figure S15. Temperature-dependent UV-*vis* absorption spectroscopy of thin film of *n*IID-310s and *n*IID-318s. Within the instrumental temperature range, the absorption peaks of 4IID-310 and *n*IID-318s (*n* = 3, 4, 6, and 8) remain almost constant below the phase transition temperature of the alkyl chains over the instrumental temperature range, suggesting that the dihedral angle of the backbone is fixed by the alkyl chains.

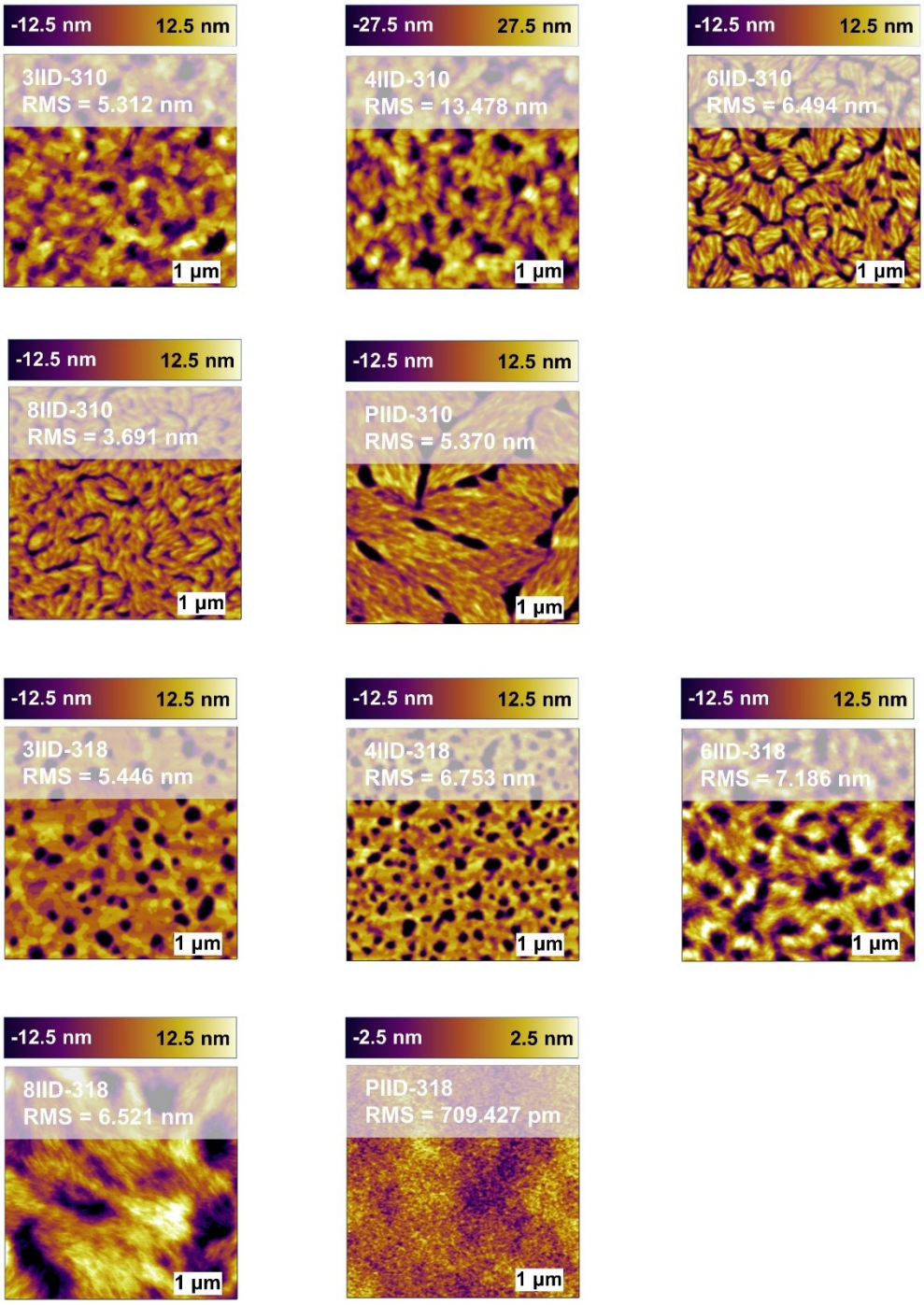

Figure S16. AFM height images of thin film of *n*IID-310s and *n*IID-318s after annealing.

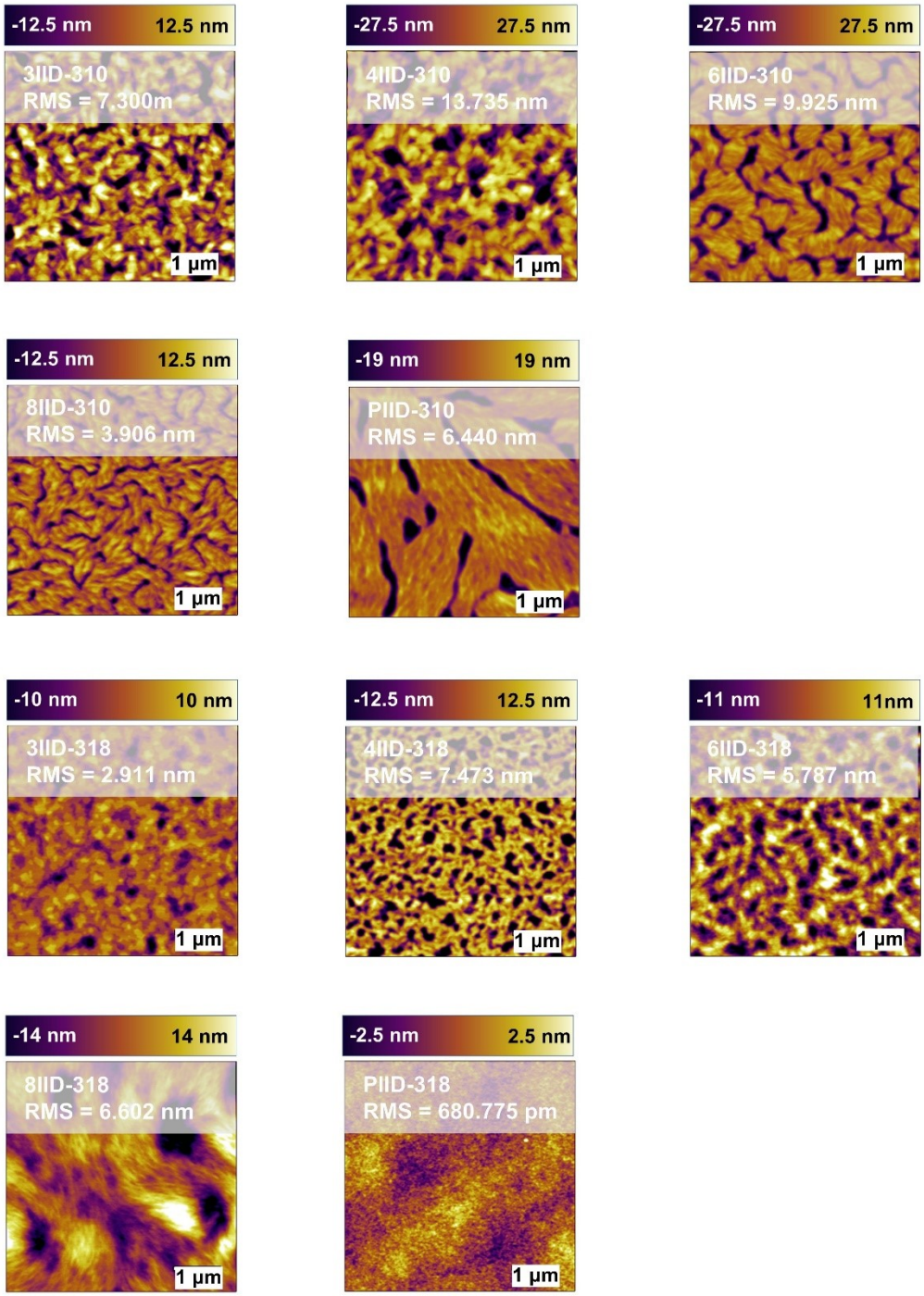

Figure S17. AFM height images of thin film of *n*IID-310s and *n*IID-318s before annealing.

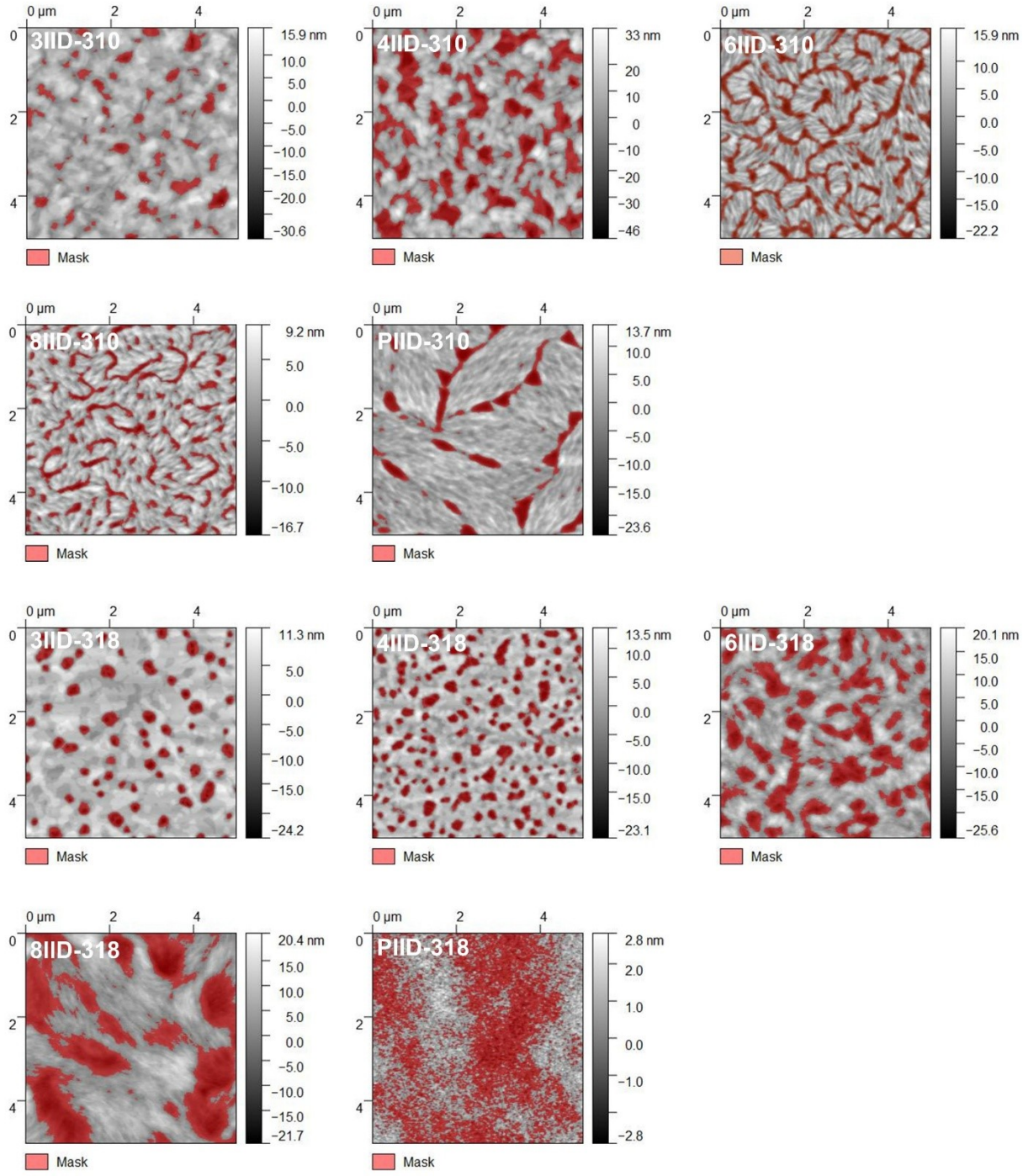

Figure S18. Mask dark region of *n*IID-310s and *n*IID-318s in thin film with threshold by 50% height.

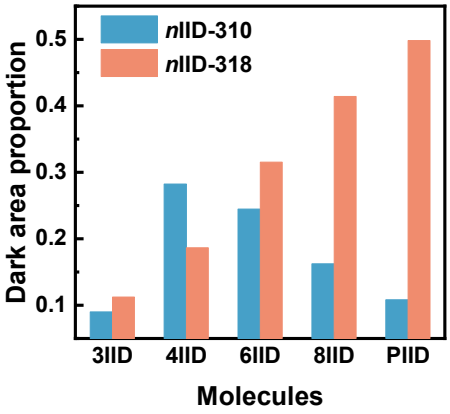

Figure S19. Dark area proportion of thin-film of *n*IID-310s and *n*IID-318.

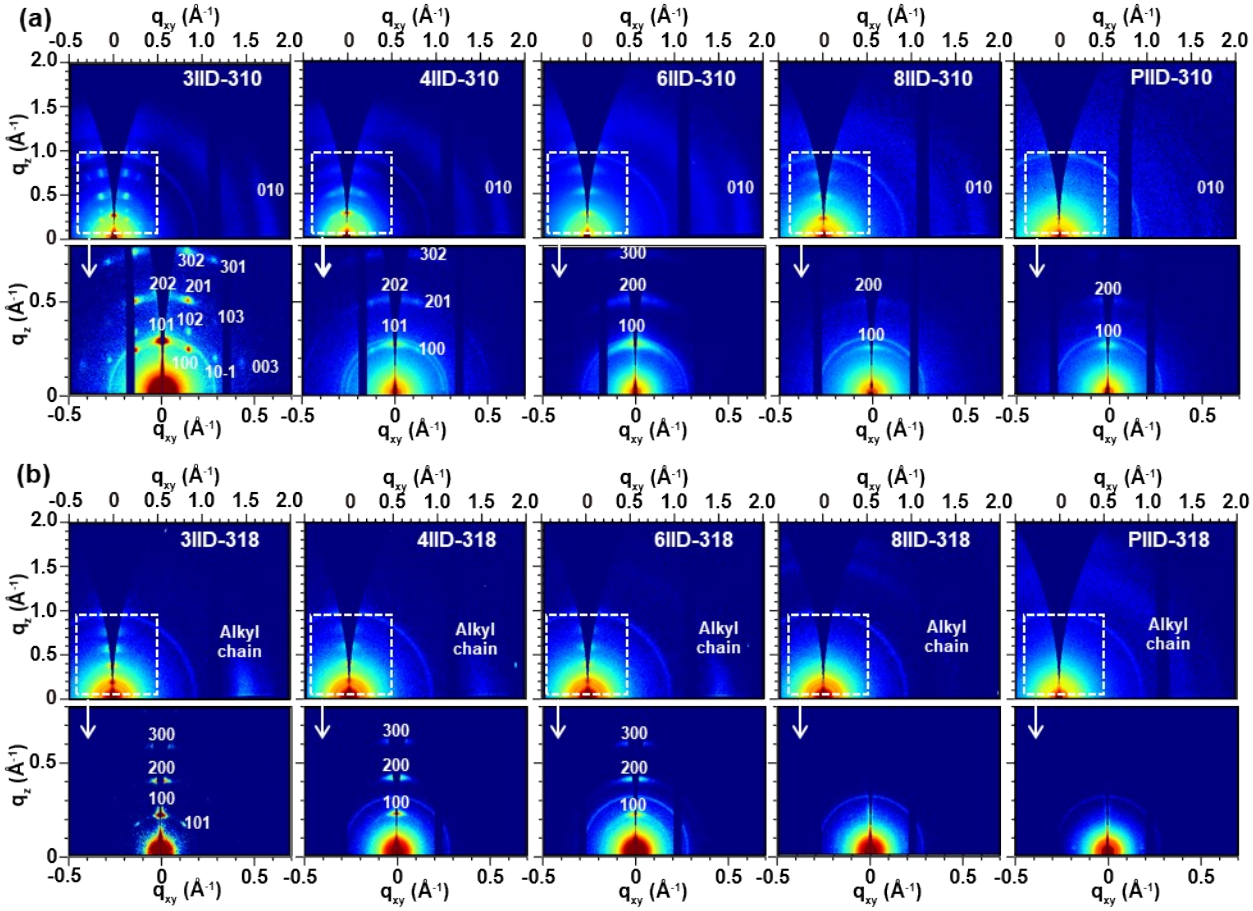

Figure S20. (a) 2D GIWAXS patterns of *n*IID-310s after transformation into reciprocal space acquired at different detector distance of the same film. (b) 2D GIWAXS patterns of *n*IID-318s after transformation into reciprocal space acquired at different detector distance of the same film. The diffraction peak observed in 3IID-310 and 4IID-310 along the q_z direction is indexed as (101) based on a monoclinic lattice model. In this lattice, the (100) and (101) planes have comparable spacings, and the conjugated backbones are arranged along the diagonal direction of the unit cell. As a result, the lamellar stacking appears as the (101) reflection along q_z, while the molecular orientation remains edge-on.

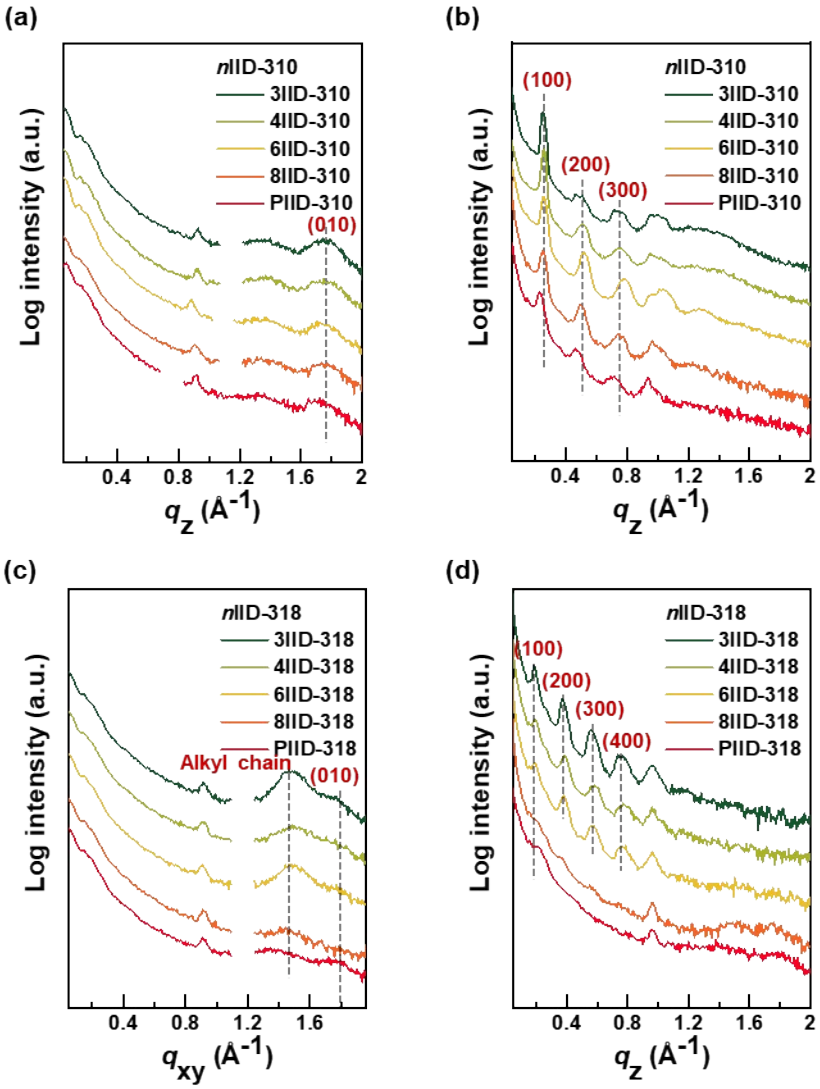

Figure S21. 1D GIWAXS plots of *n*IID-310s and *n*IID-318s in thin films. Diffraction intensity was integrated along the radial direction and plotted against the scattering vector.

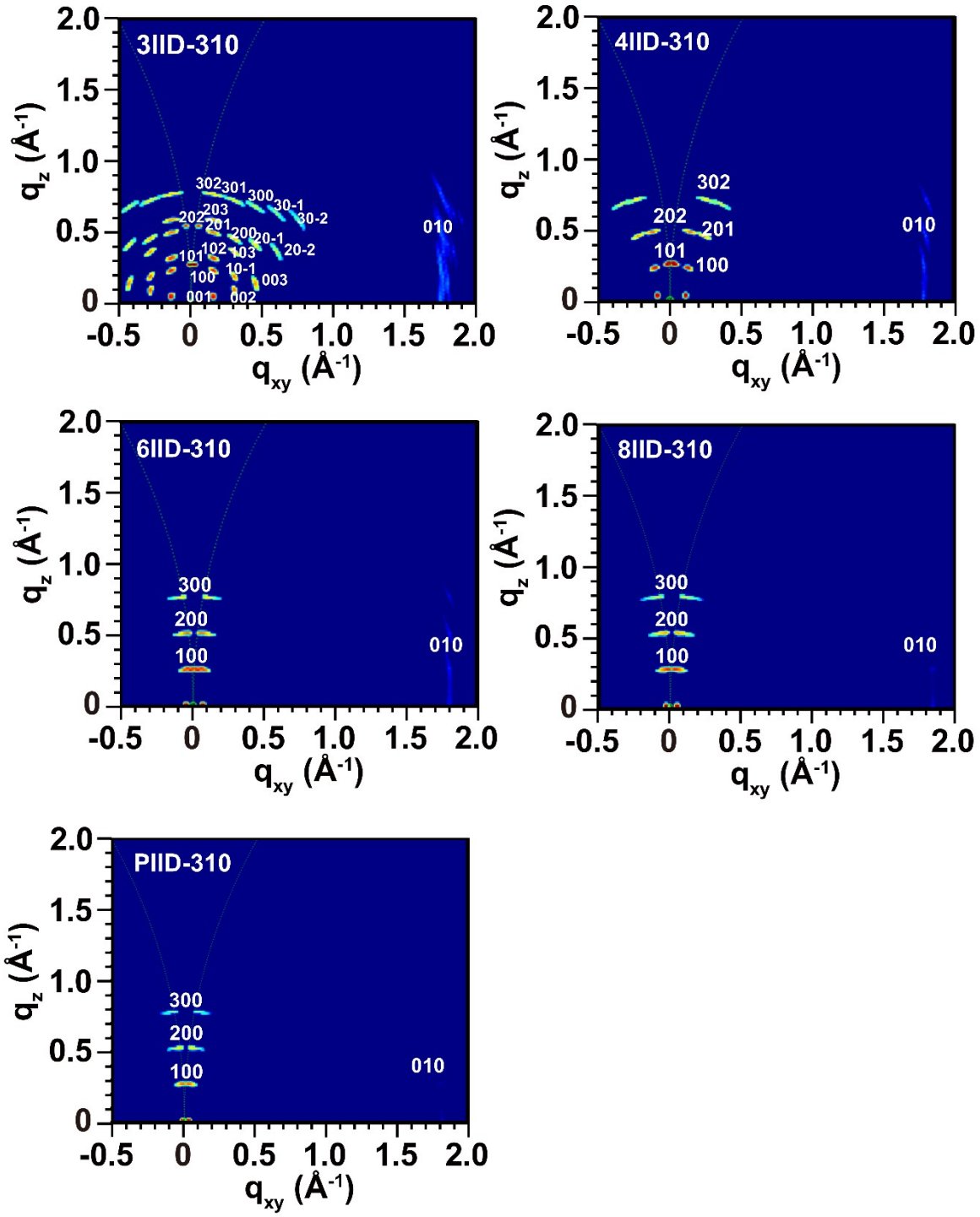

Figure S22. Simulation of 2D GIWAXS of *n*IID-310s in thin films according to the fitting unit cell structure.

Table S2. Fitting unit cell structure of 3IID-310, 4IID-310, 6IID-310, 8IID-310, and PIID-310.

	3IID-310	**4IID-310**	**6IID-310**	**8IID-310**	**PIID-310**
Lattice type	Monoclinic system	Monoclinic system	Triclinic system	Triclinic system	Triclinic system
a (Å)	24.26	25.20	24.61	24.40	24.38
b (Å)	3.58	3.52	3.51	3.49	3.52
c (Å)	42.23	60.59	110.24	145.00	278.61
α (°)	90.00	90.00	84.01	76.93	78.83
B (°)	73.00	78.79	88.62	86.23	88.47
γ (°)	90.00	90.00	89.64	86.00	92.42

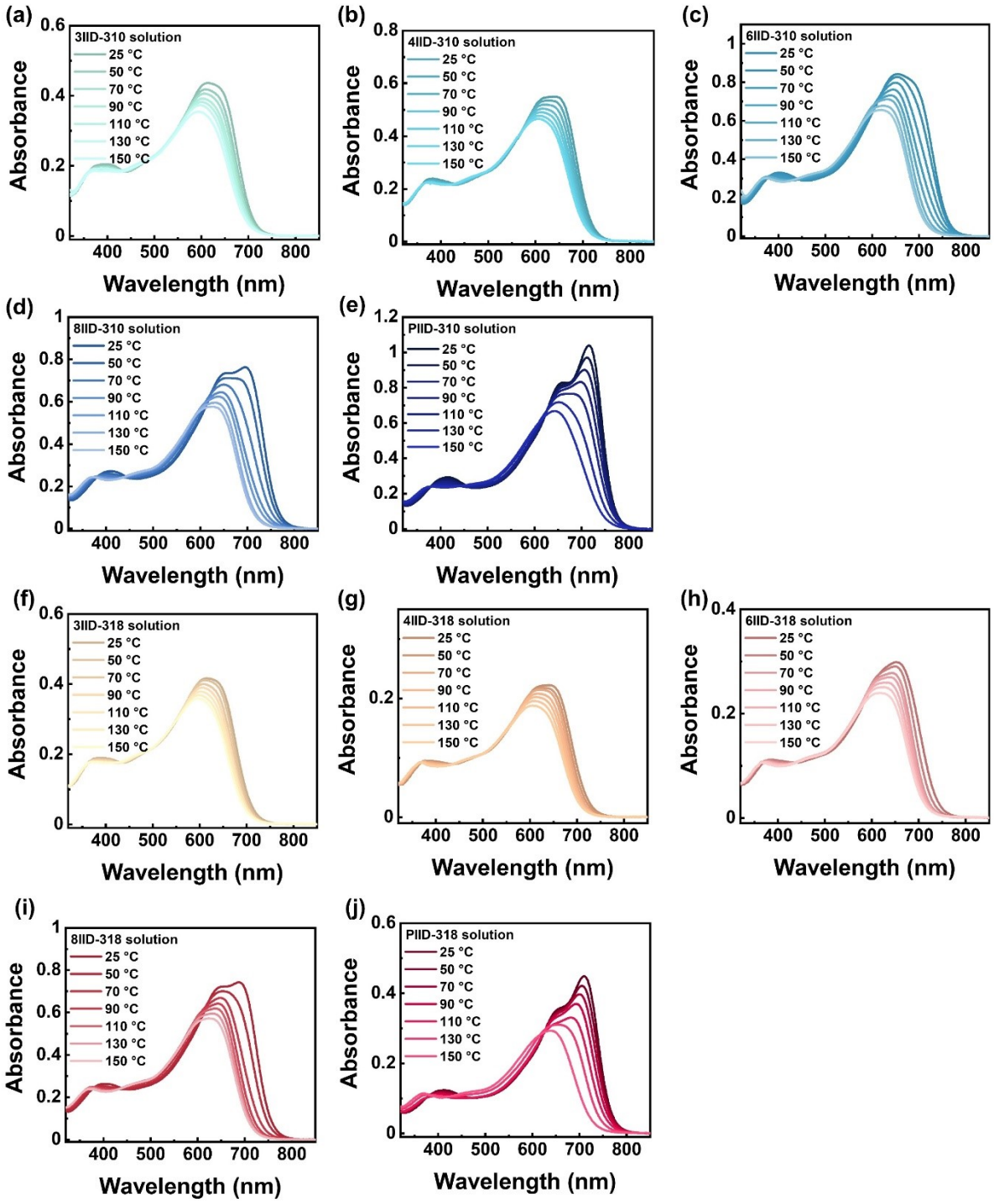

Figure S23. Temperature-dependent UV-*vis* absorption spectroscopy of *n*IID-310s and *n*IID-318s in *o*DCB solution.

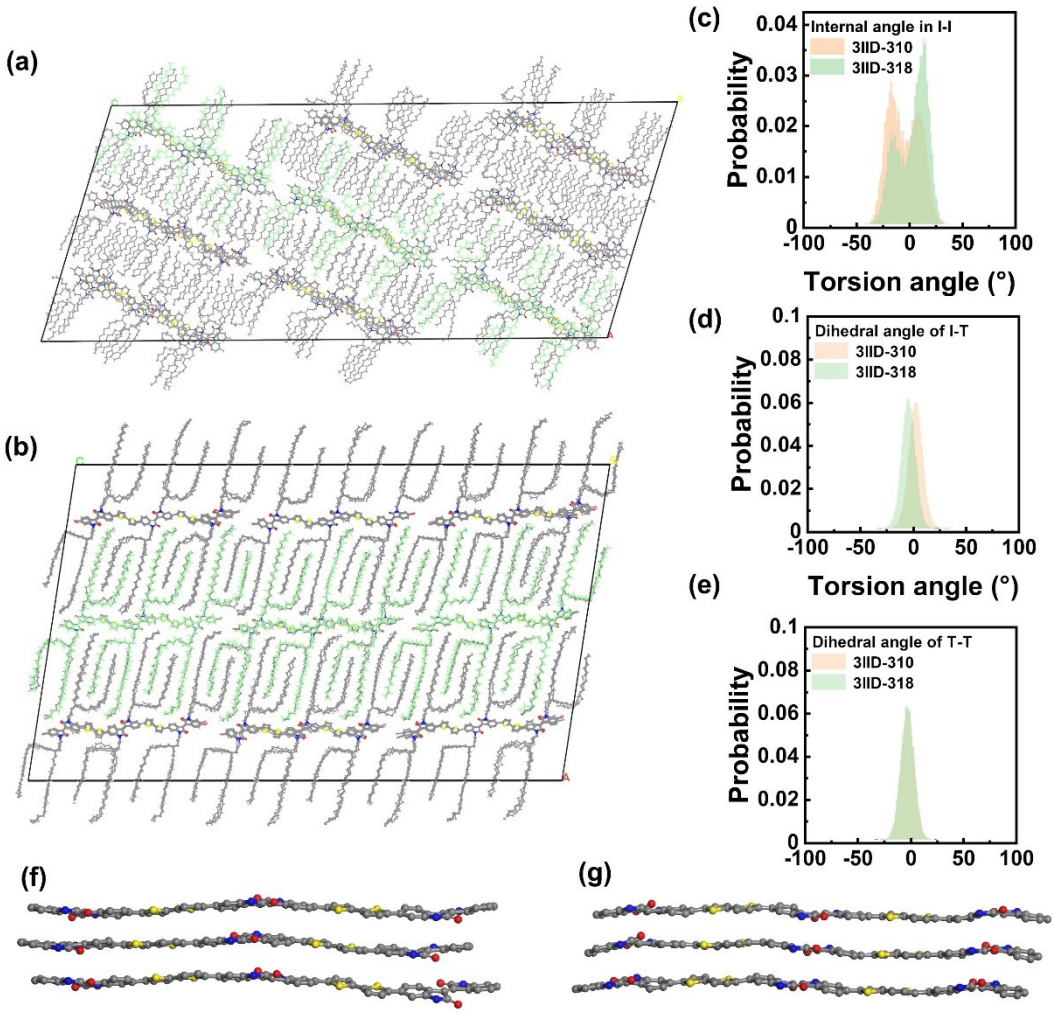

Figure S24. Equilibrated snapshots of 3IID-310 and 3IID-318 from molecular dynamics simulations of the 3 × 3 × 3 supercell. (a) 3IID-310. (b) 3IID-318. (c–e) Dihedral angle distribution of 3IID-310 and 3IID-s318 analyzed from equilibrated process. (f) side view of 3IID-310 extracted from supercell. (g) side view of 3IID-318 extracted from supercell.

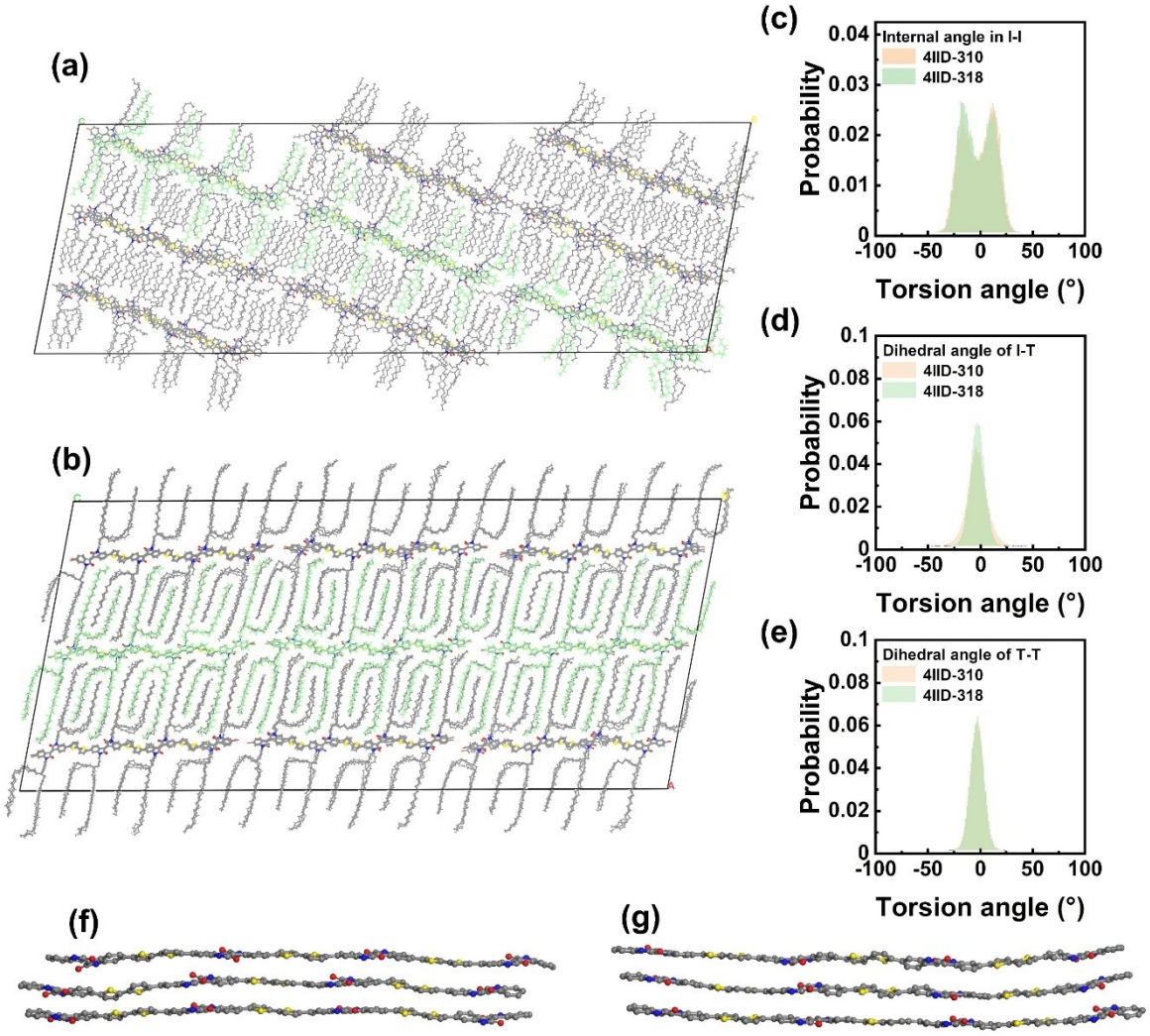

Figure S25. Equilibrated snapshots of 4IID-310 and 4IID-318 from molecular dynamics simulations of the 3 × 3 × 3 supercell. (a) 4IID-310. (b) 4IID-318. (c–e) Dihedral angle distribution of 4IID-310 and 4IID-318 analyzed from equilibrated process. (f) side view of 4IID-310 extracted from supercell. (g) side view of 4IID-318 extracted from supercell.

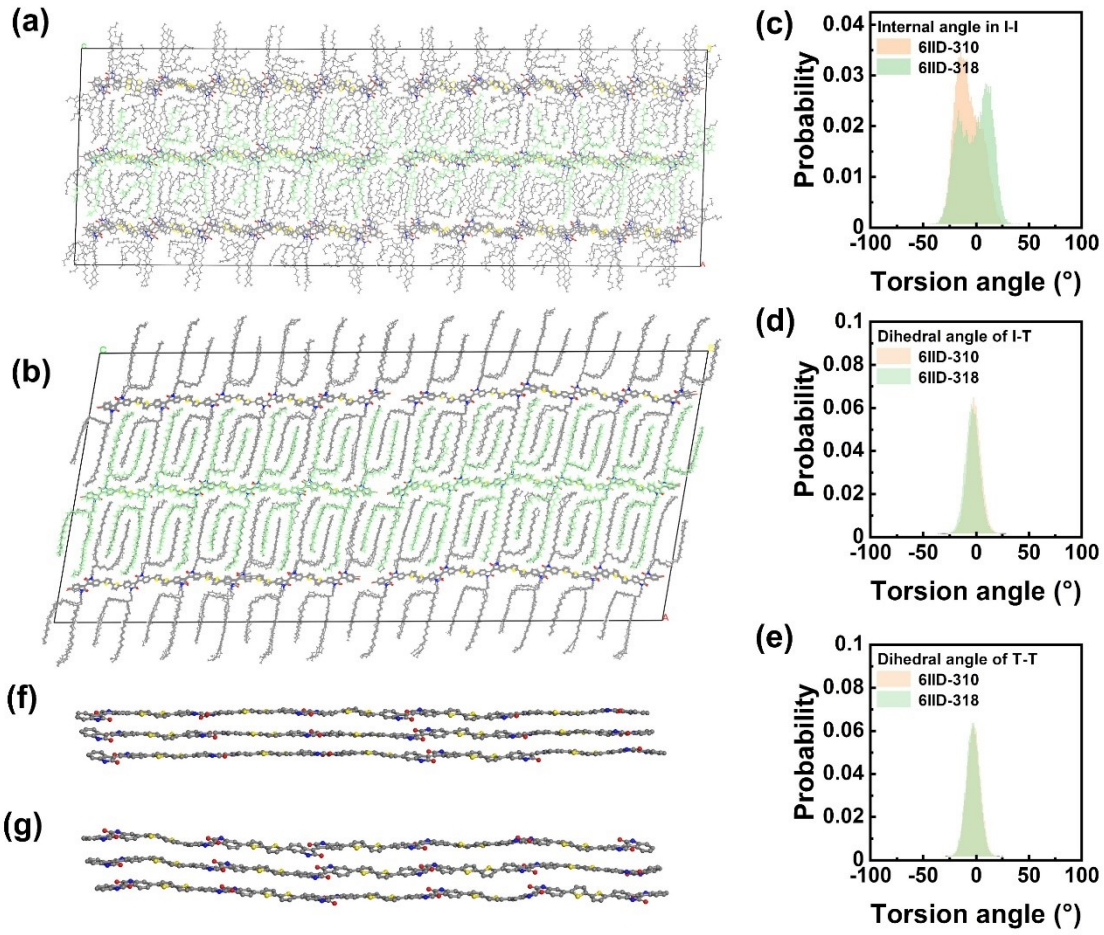

Figure S26. Equilibrated snapshots of 6IID-310 and 6IID-318 from molecular dynamics simulations of the 3 × 3 × 2 supercell. (a) 6IID-310. (b) 6IID-318. (c–e) Dihedral angle distribution of 6IID-310 and 6IID-318 analyzed from equilibrated process. (f) side view of 6IID-310 extracted from supercell. (g) side view of 6IID-318 extracted from supercell.

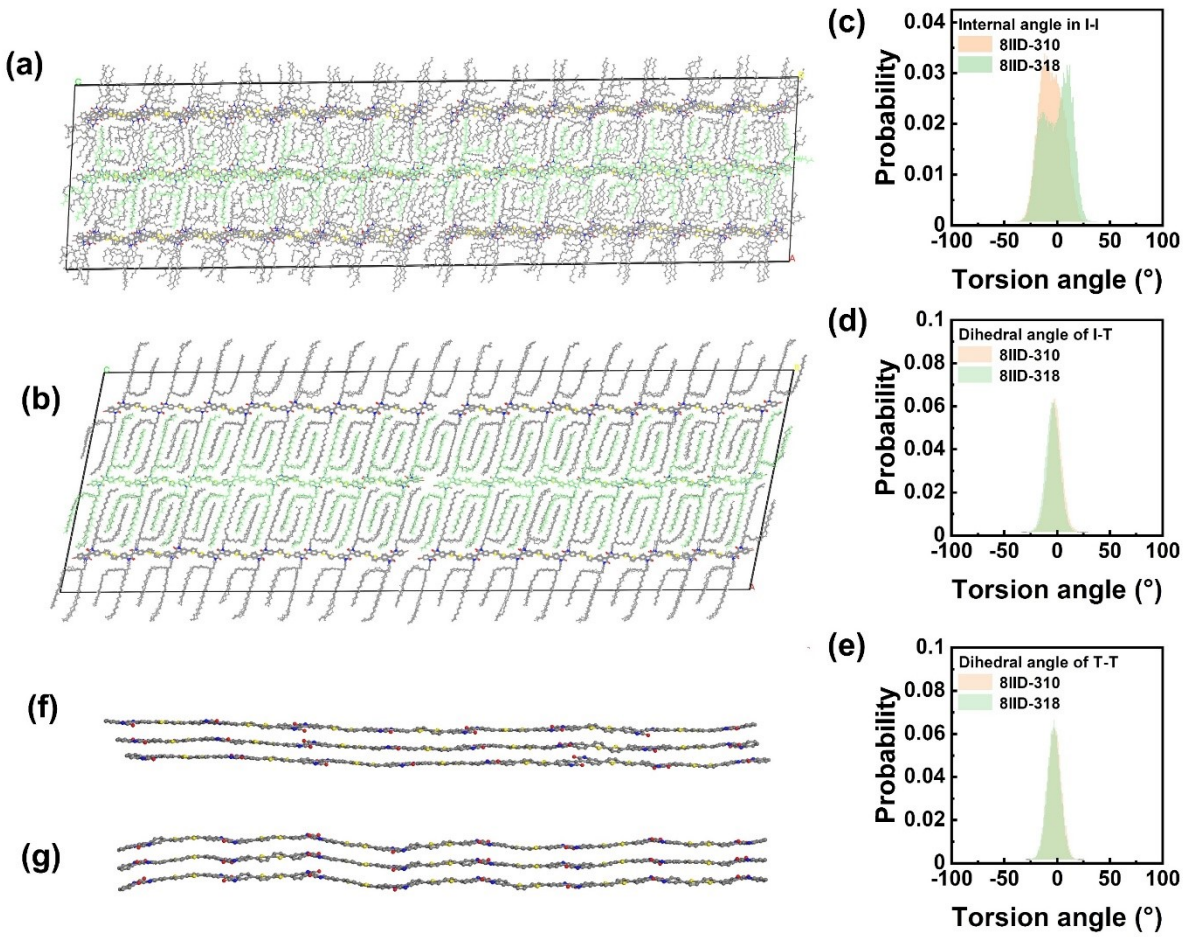

Figure S27. Equilibrated snapshots of 8IID-310 and 8IID-318 from molecular dynamics simulations of the 3 × 3 × 2 supercell. (a) 8IID-310. (b) 8IID-318. (c–e) Dihedral angle distribution of 8IID-310 and 8IID-318 analyzed from equilibrated process. (f) side view of 8IID-310 extracted from supercell. (g) side view of 8IID-318 extracted from supercell.

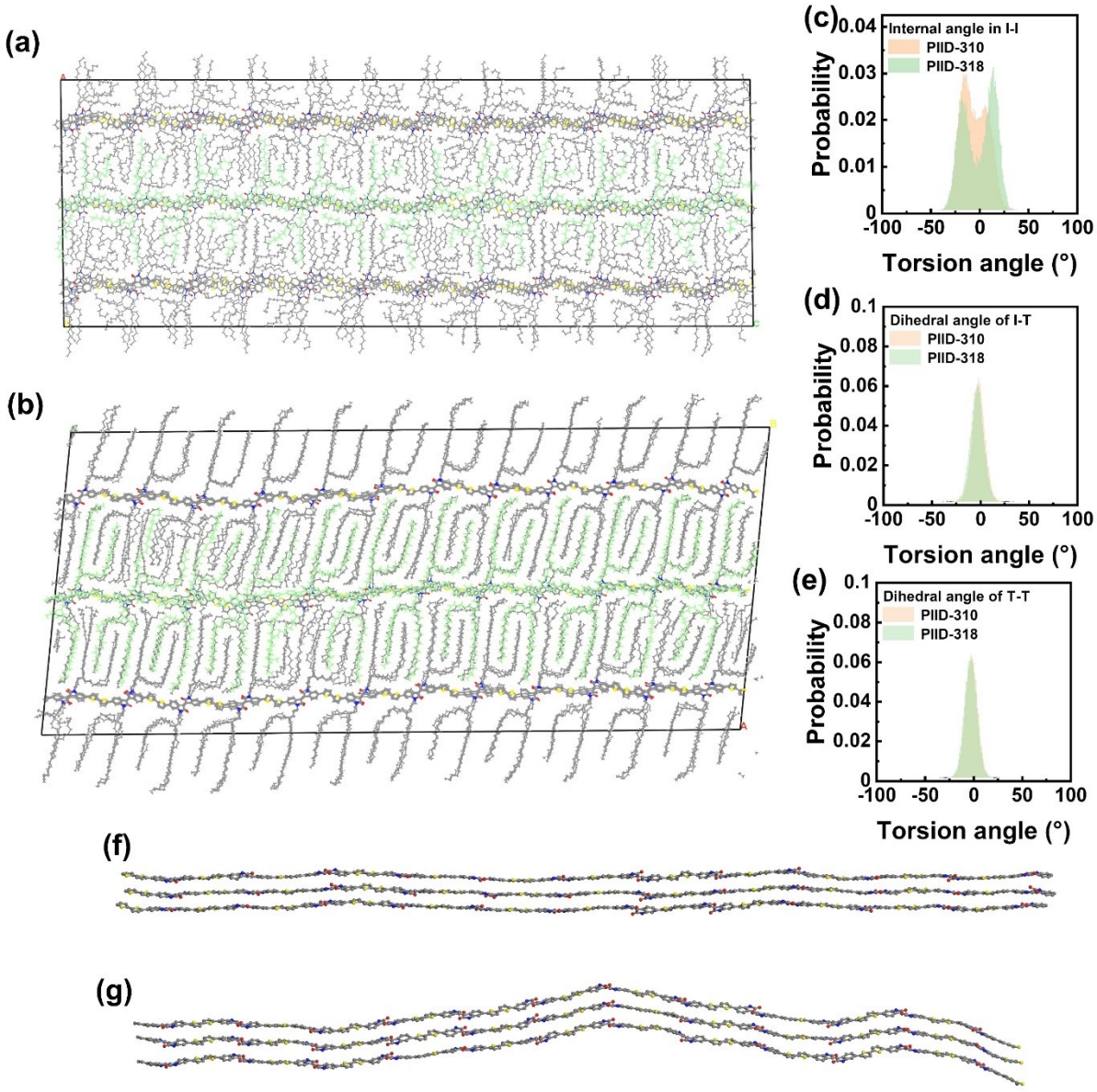

Figure S28. Equilibrated snapshots of PIID-310 and PIID-318 from molecular dynamics simulations of the 3 × 3 × 2 supercell. (a) PIID-310. (b) PIID-318. (c–e) Dihedral angle distribution of PIID-310 and PIID-318 analyzed from equilibrated process. (f) side view of PIID-310 extracted from supercell. (g) side view of PIID-318 extracted from supercell.

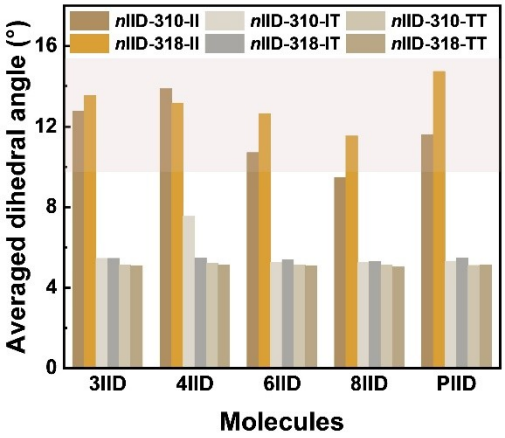

Figure S29. Mean dihedral angle of different molecules extracted from molecular dynamics simulations.

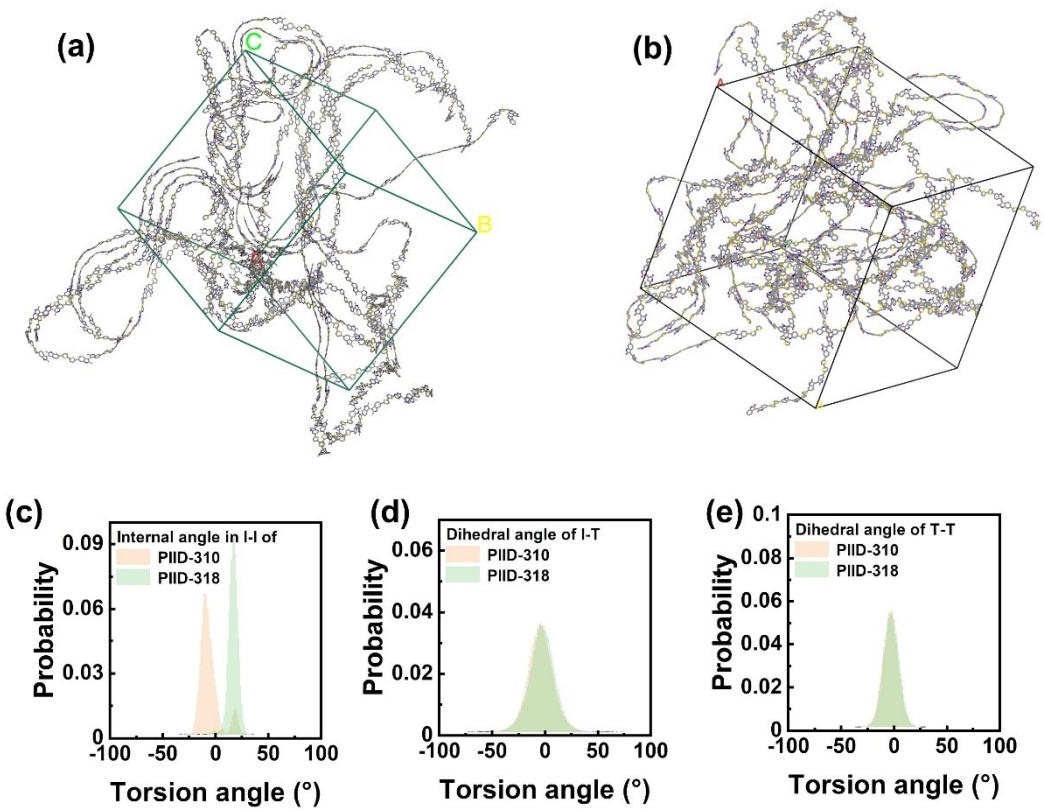

Figure S30. Equilibrated snapshots of PIID-310 and PIID-318 from molecular dynamics simulations of amorphous cell. (a) PIID-310. (b) PIID-318. (c–e) Dihedral angle distribution of PIID-310 and PIID-318 analyzed from equilibrated process.

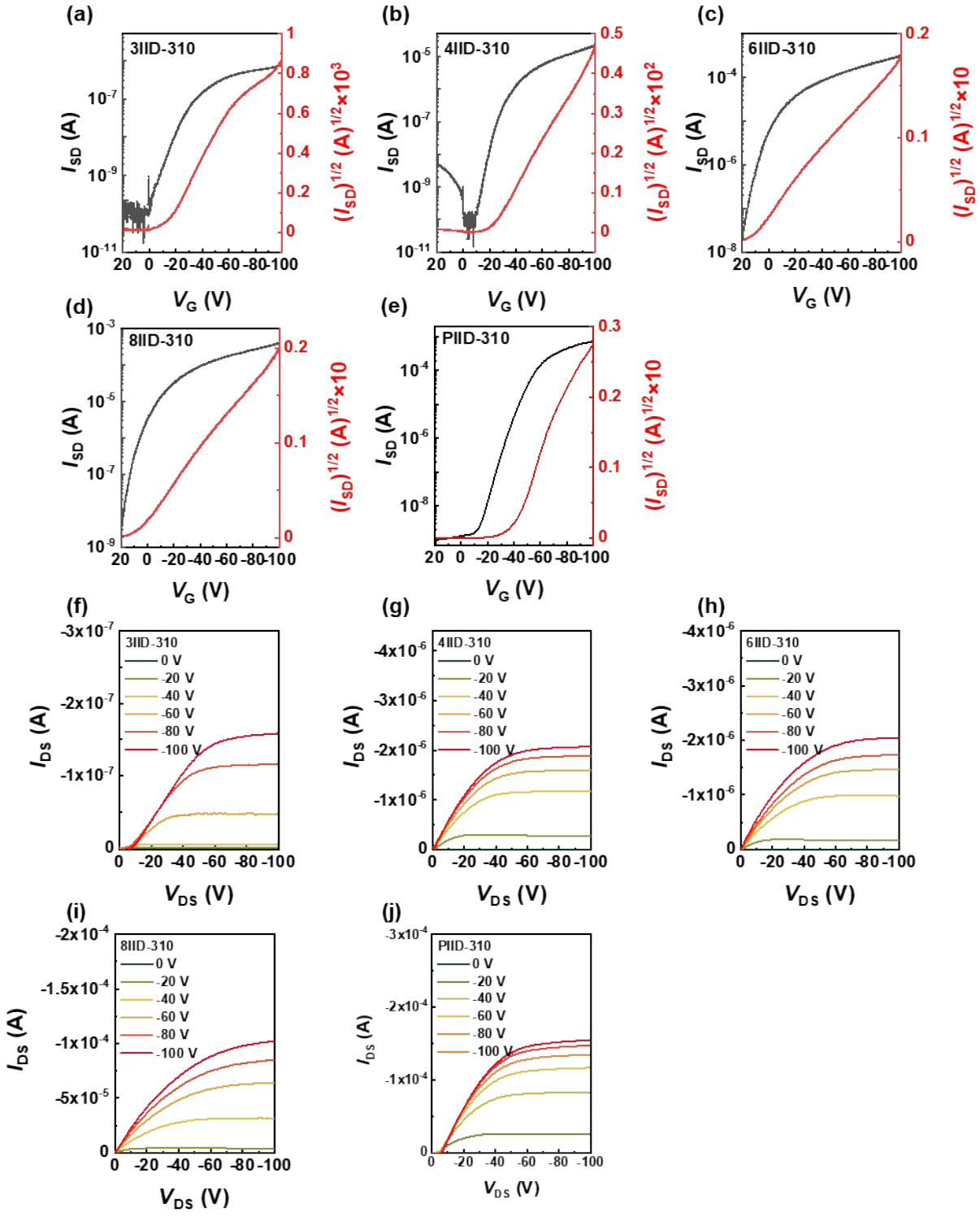

Figure S31. Transfer characteristics and output characteristics of transistors of *n*IID-310s. The channel width and length are 1200 and 30 μm, respectively. (a-e) transfer characteristics curves. (f-j) output characteristics curves.

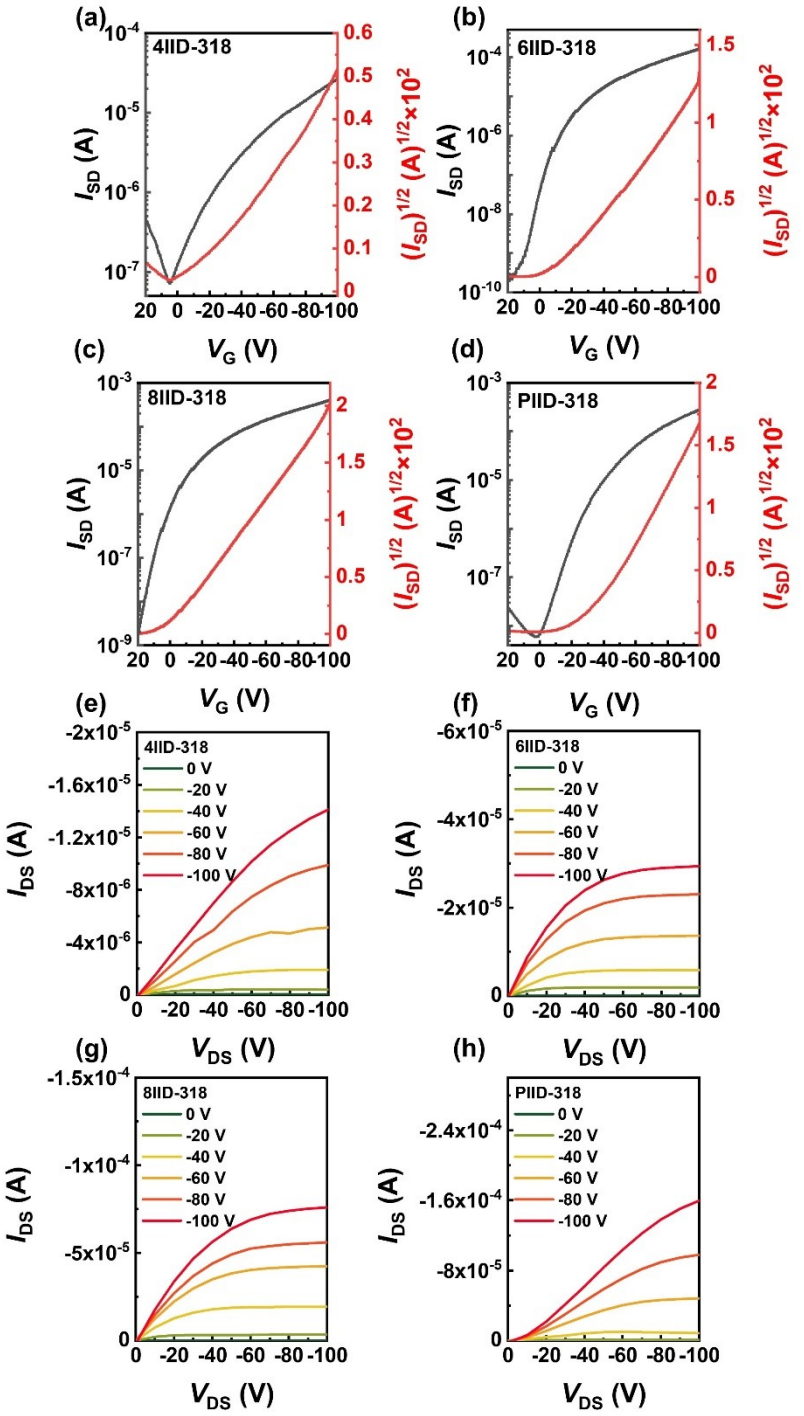

Figure S32. Transfer characteristics and output characteristics of transistors of *n*IID-318s. The channel width and length are 1200 and 30 μm, respectively. (a-d) transfer characteristics curves. (e-h) output characteristics curves.

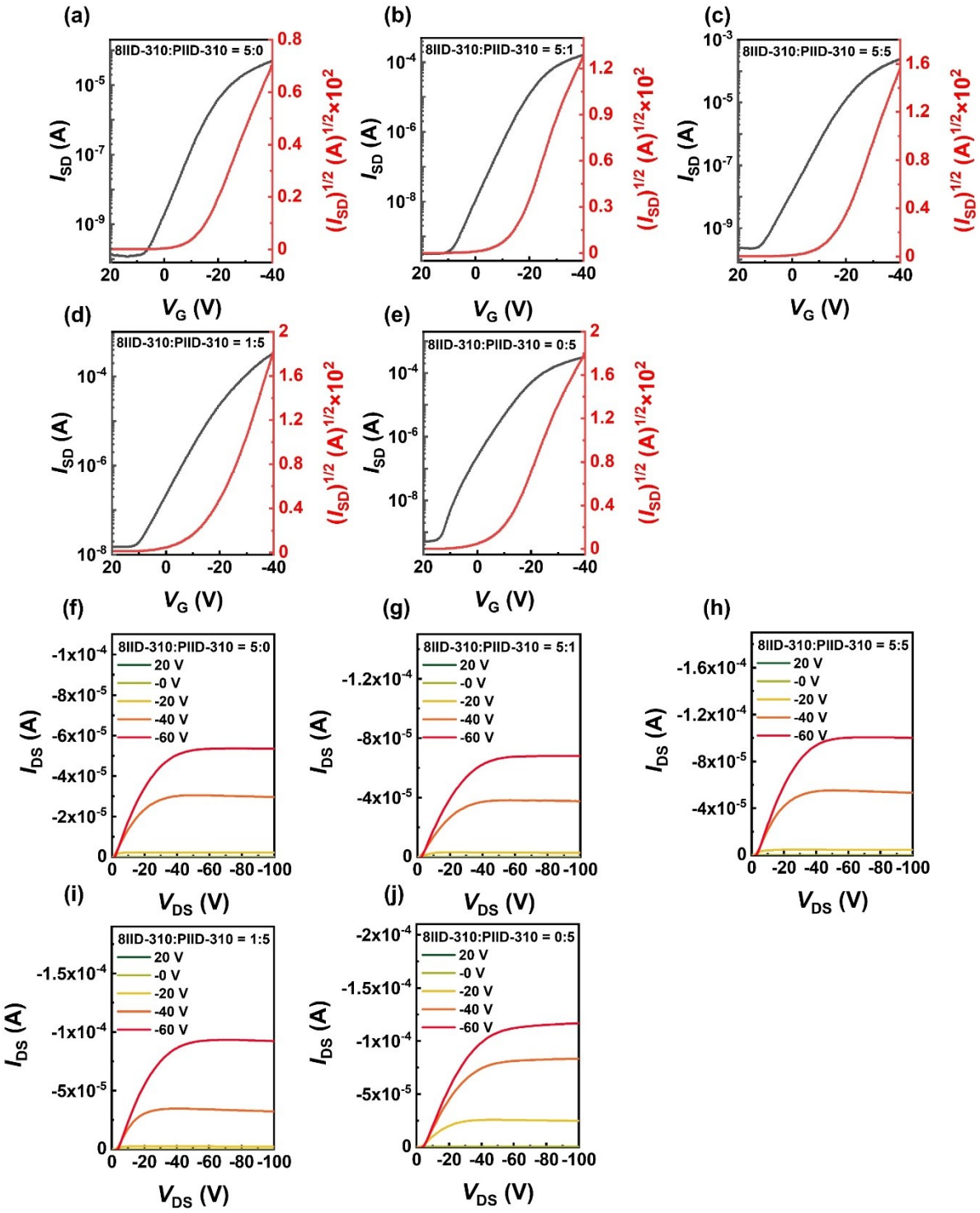

Figure S33. Transfer characteristics and output characteristics of transistors of blending 8IID-310 and PIID-310 with different weight ratio. The channel width and length are 1200 and 30 μm, respectively. (a-e) transfer characteristics curves. (f-j) output characteristics curves.

3. ^{1}H and ^{13}C NMR spectra of all compounds.

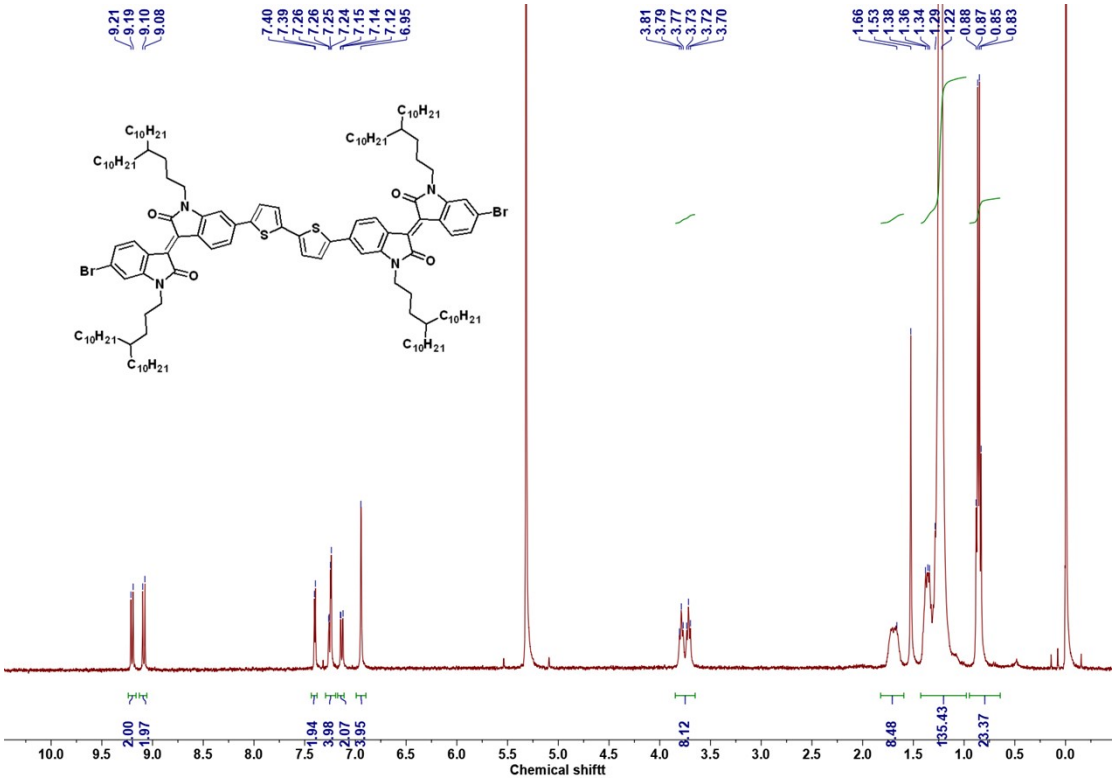

Figure S34. ^{1}H-NMR spectrum of 2IID-310 in $C_2D_2Cl_4$ (400 MHz).

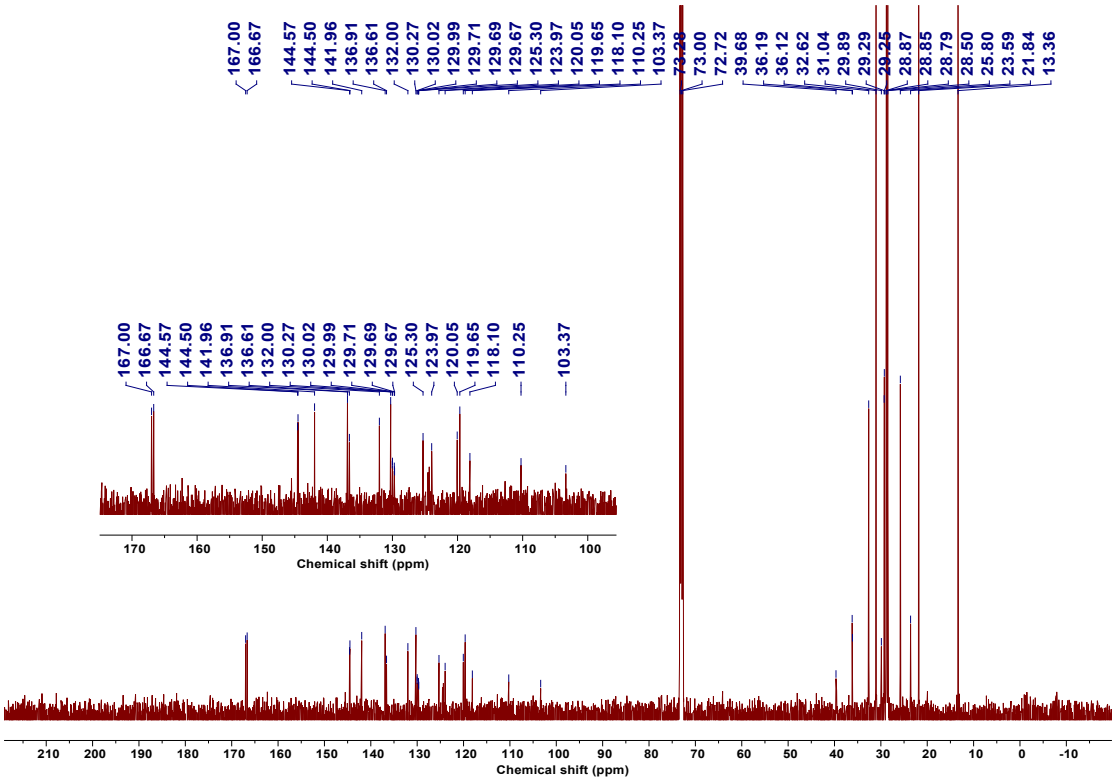

Figure S35. ^{13}C-NMR spectrum of 2IID-310 in $C_2D_2Cl_4$ (101 MHz).

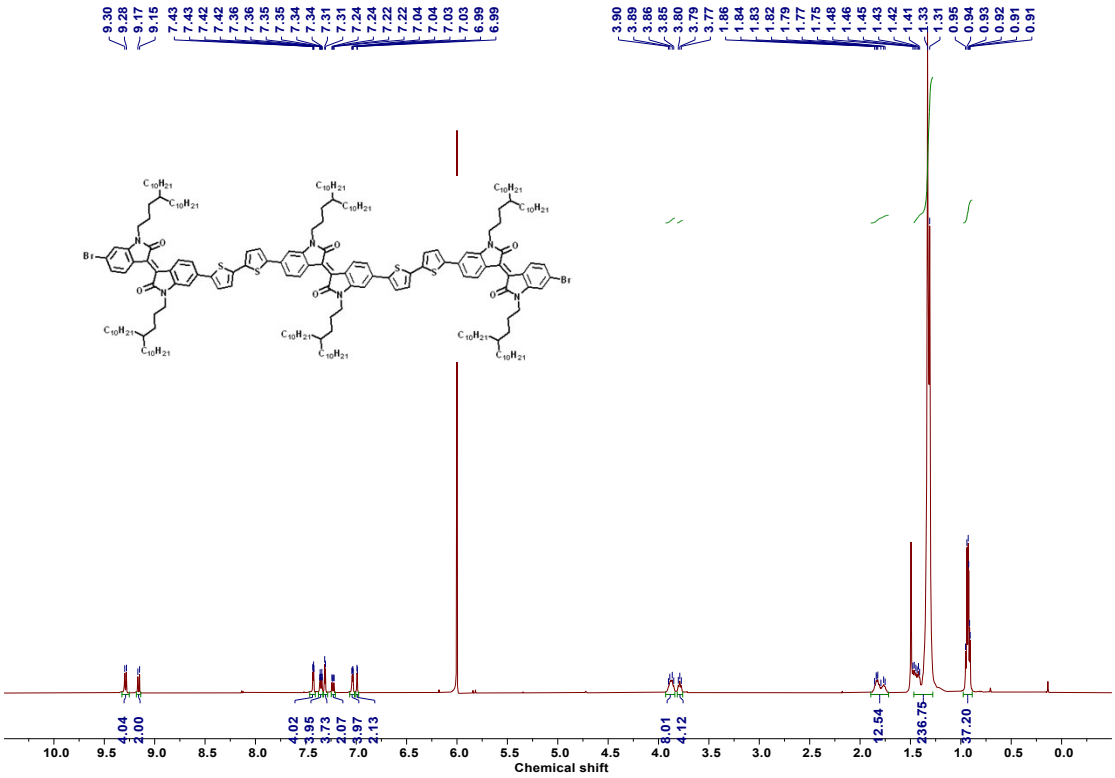

Figure S36. ^{1}H-NMR spectrum of 3IID-310 in $C_2D_2Cl_4$ (363K, 500 MHz).

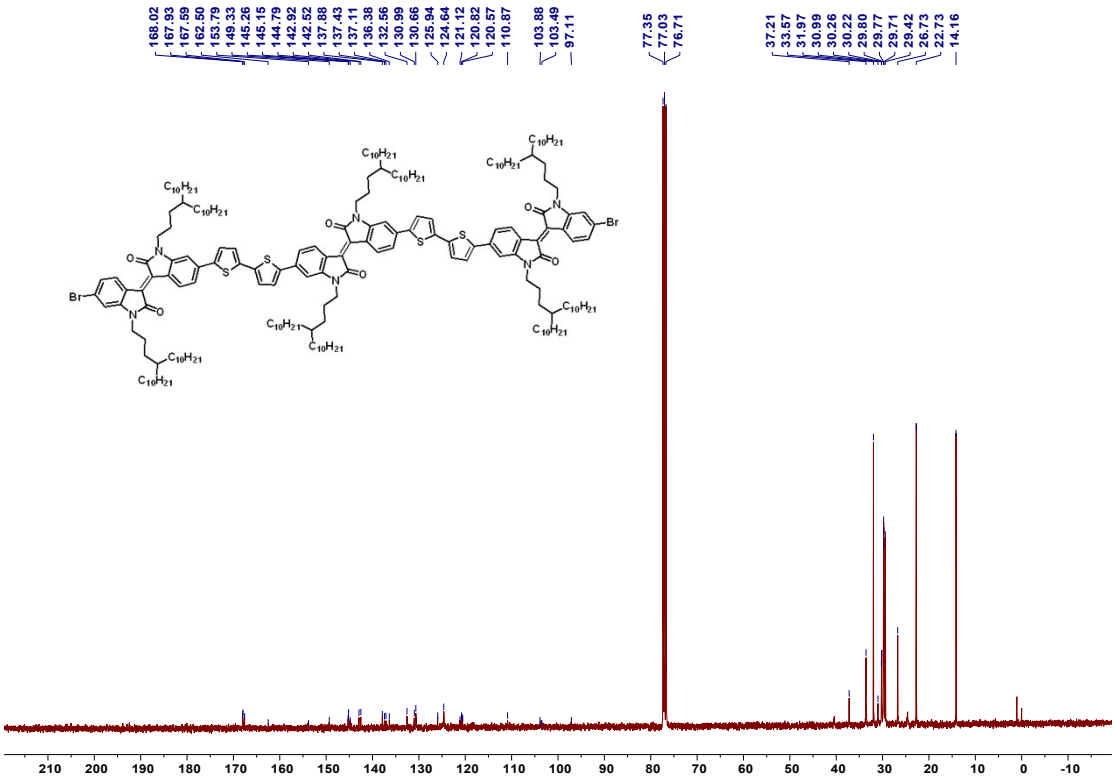

Figure S37. ^{13}C-NMR spectrum of 3IID-310 in $CDCl_3$ (101 MHz).

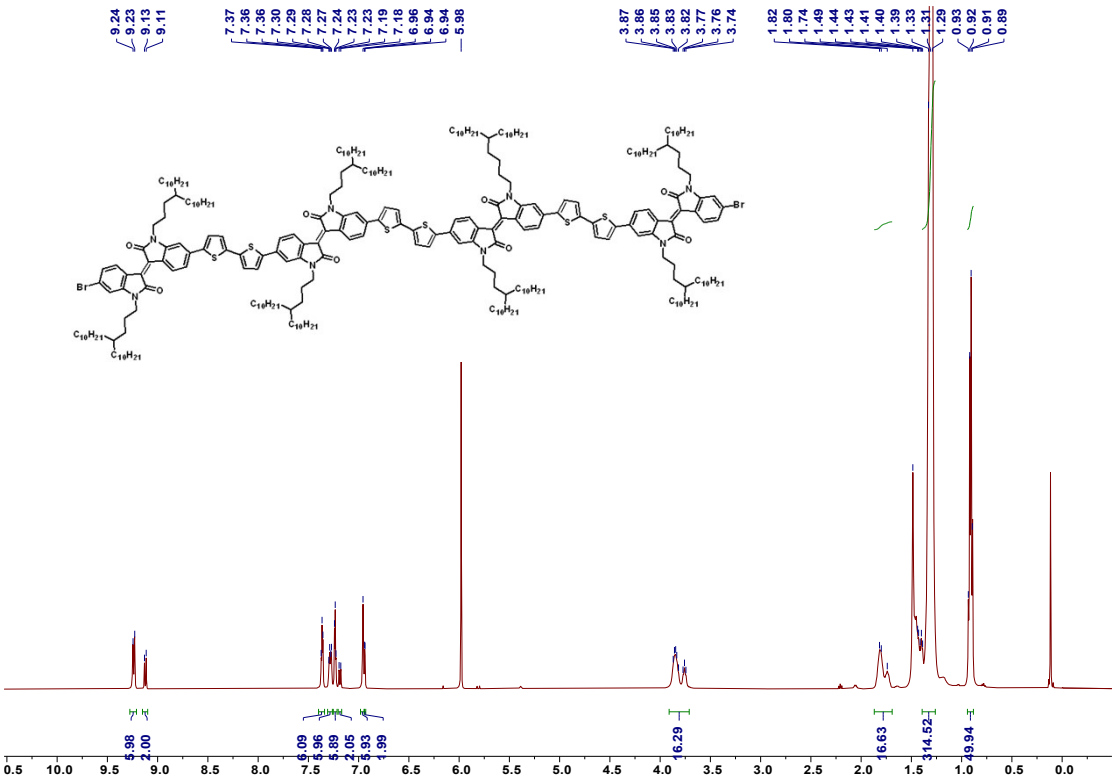

Figure S38. ^{1}H-NMR spectrum of 4IID-310 in $C_2D_2Cl_4$ (363 K, 500 MHz).

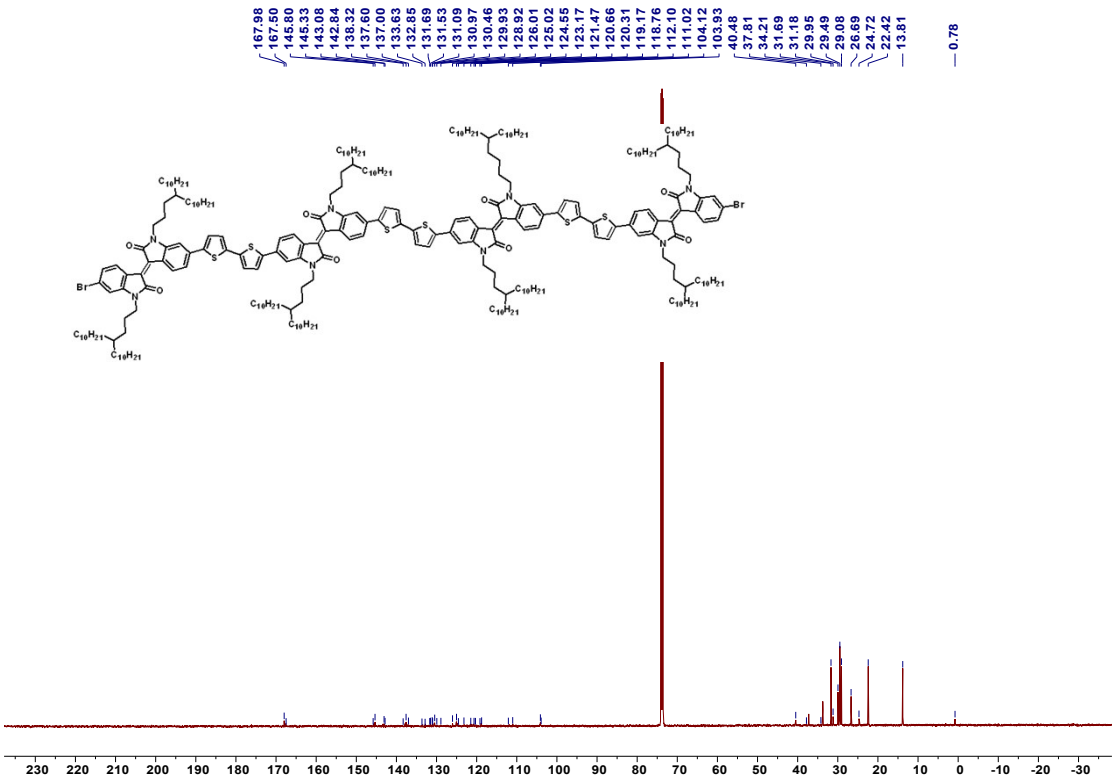

Figure S39. ^{13}C-NMR spectrum of 4IID-310 in $C_2D_2Cl_4$ (363K, 126 MHz).

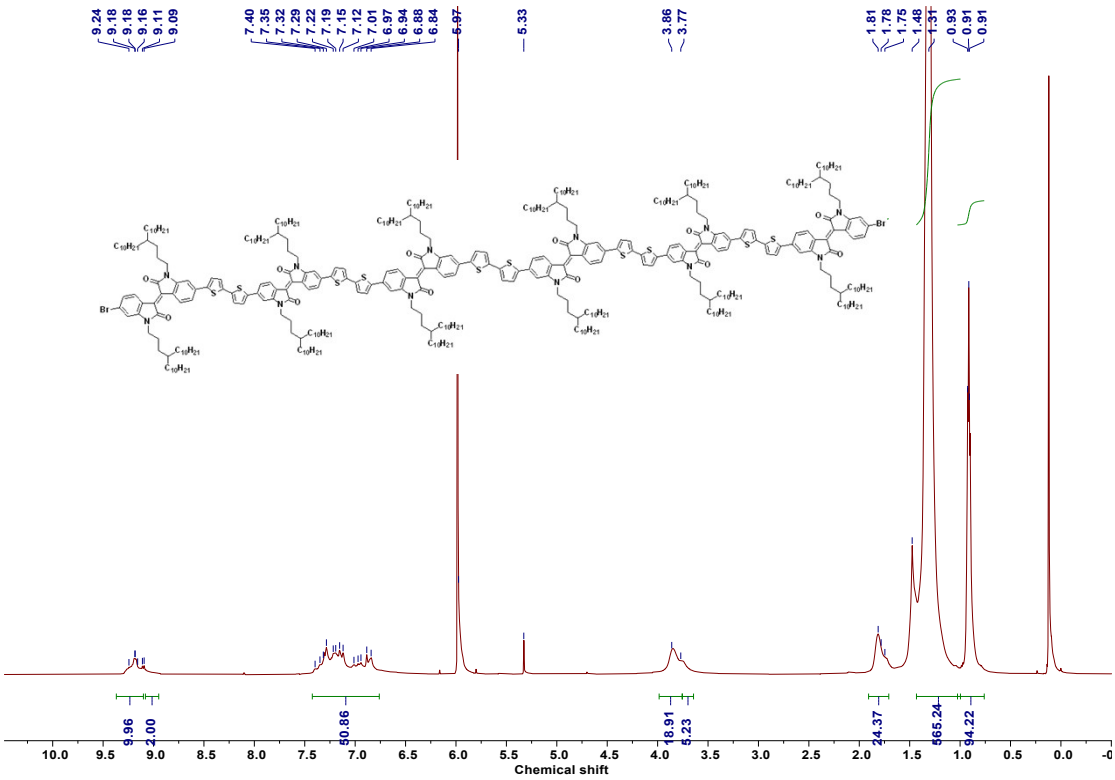

Figure S40. ^{1}H-NMR spectrum of 6IID-310 in $C_2D_2Cl_4$ (363K, 500 MHz).

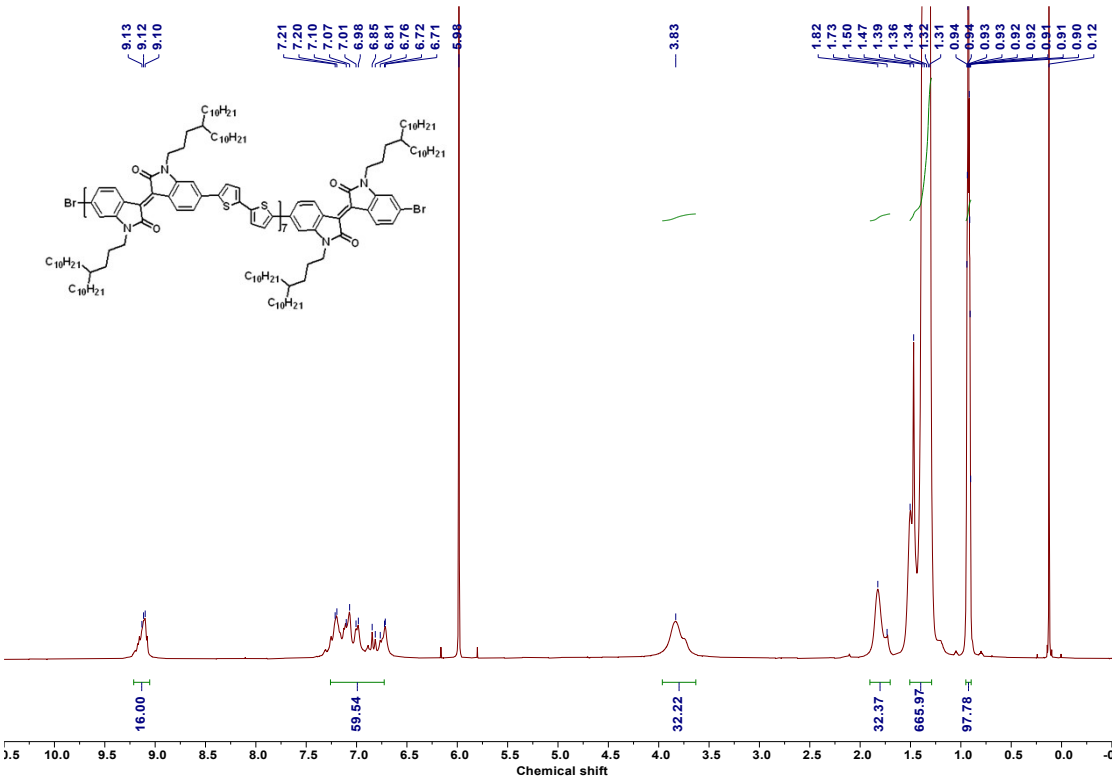

Figure S41. ^{1}H-NMR spectrum of 8IID-310 in $C_2D_2Cl_4$ (363 K, 500 MHz).

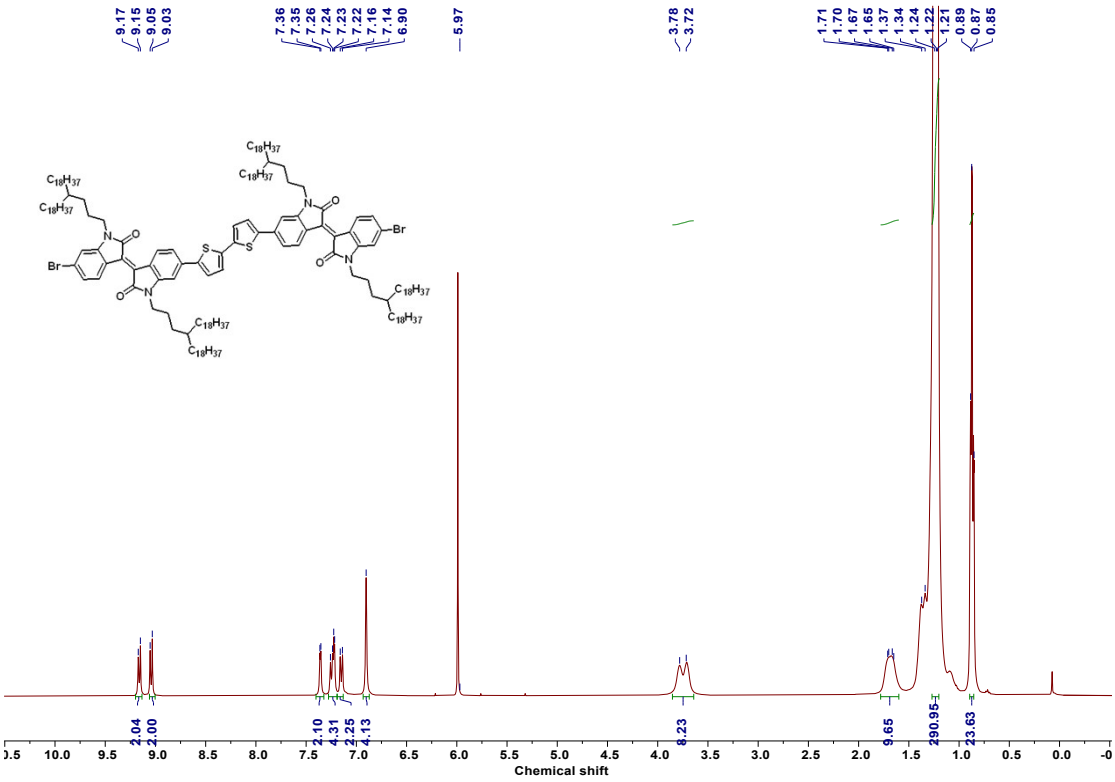

Figure S42. ^{1}H-NMR spectrum of 2IID-318 in $C_2D_2Cl_4$ (400 MHz).

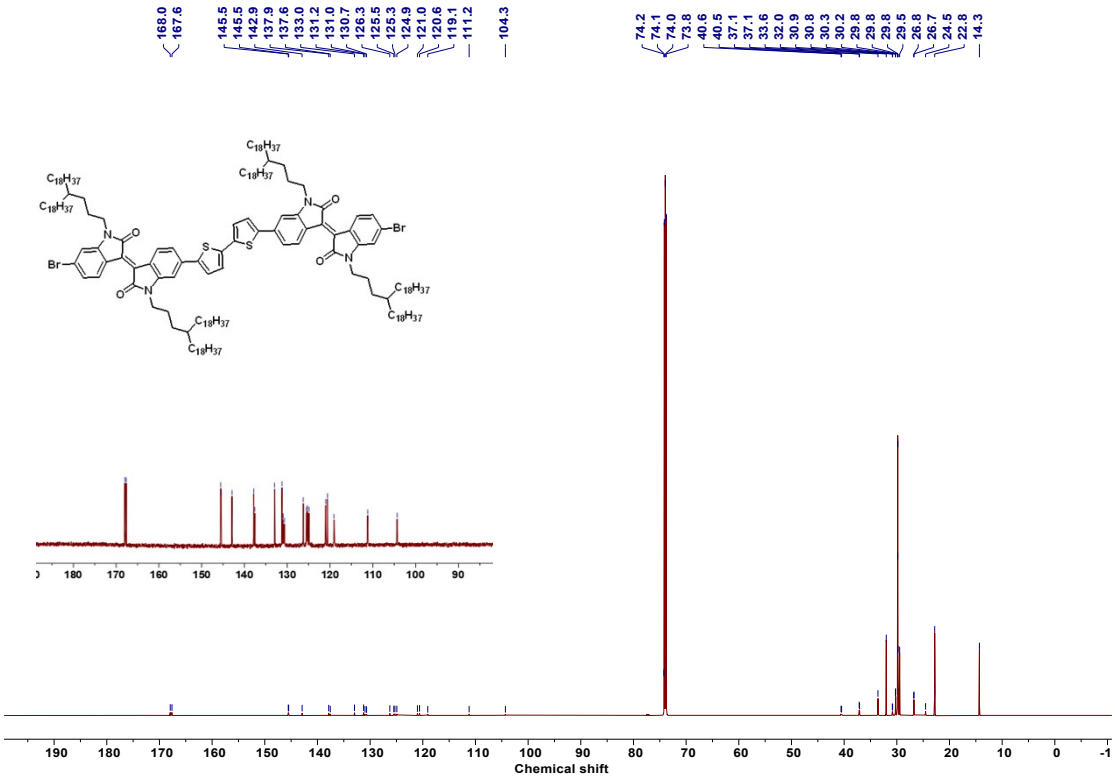

Figure S43. ^{13}C-NMR spectrum of 2IID-318 in $C_2D_2Cl_4$ (151 MHz).

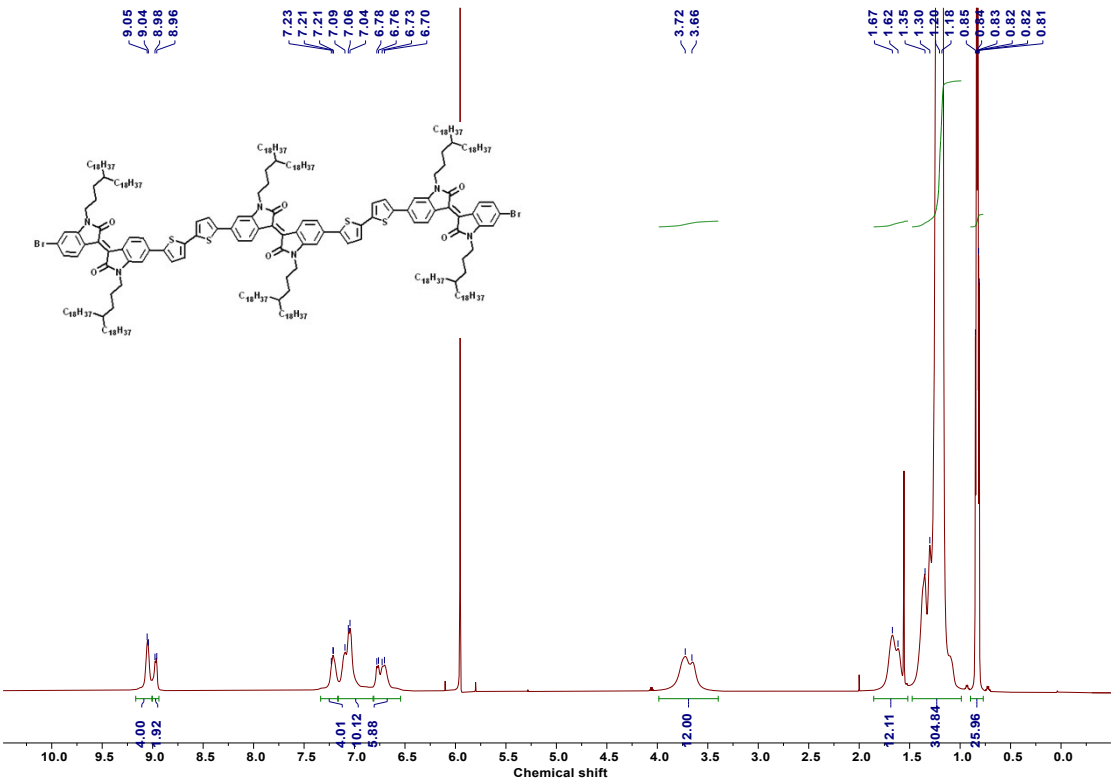

Figure S44. ^{1}H-NMR spectrum of 3IID-318 in $C_2D_2Cl_4$ (400 MHz).

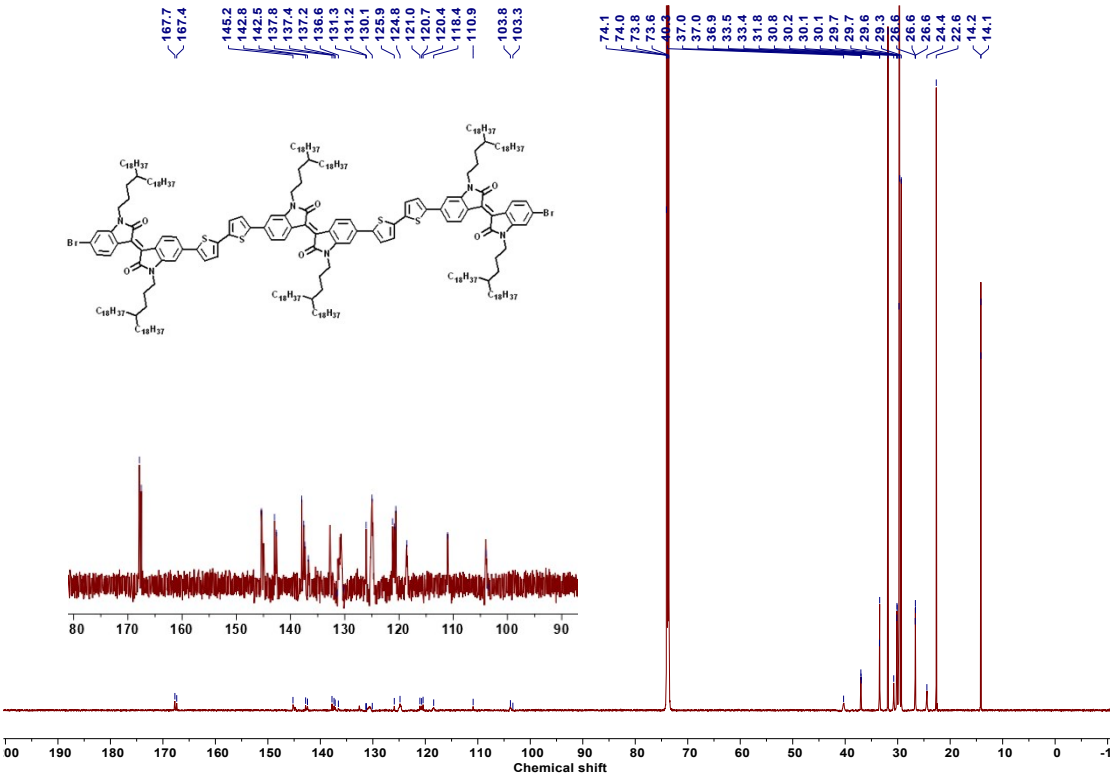

Figure S45. ^{13}C-NMR spectrum of 3IID-318 in $C_2D_2Cl_4$ (151 MHz).

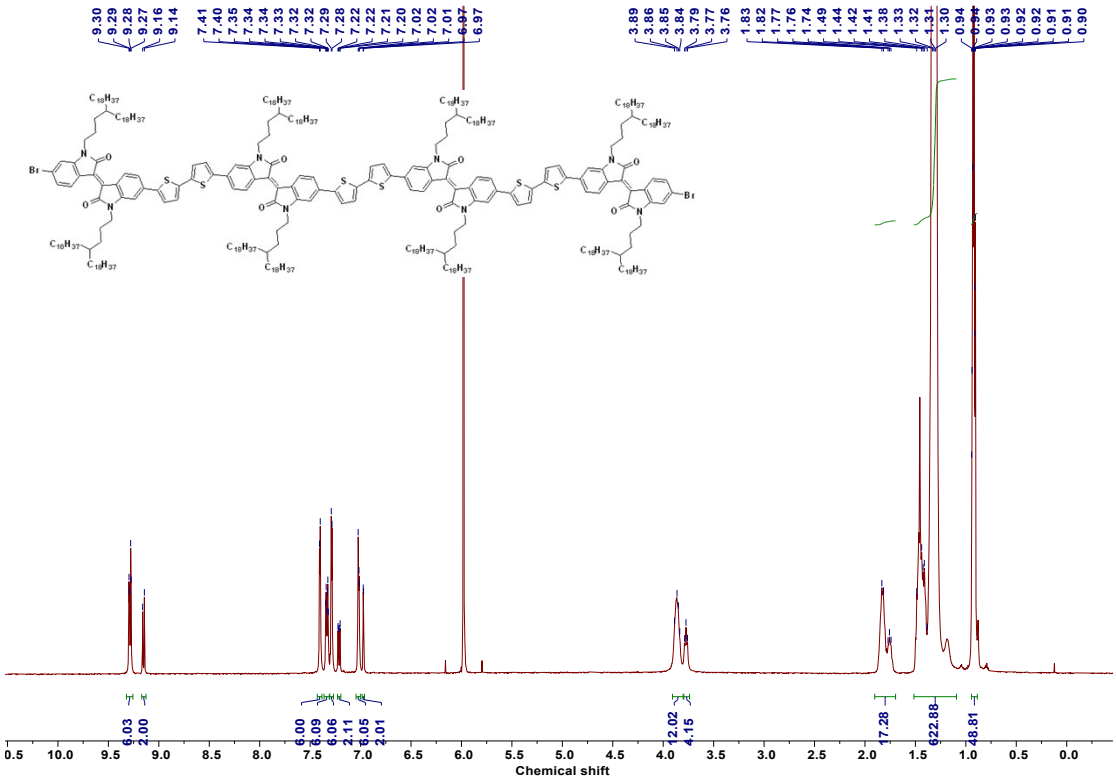

Figure S46. ^{1}H-NMR spectrum of 4IID-318 in $C_2D_2Cl_4$ (363 K, 500 MHz).

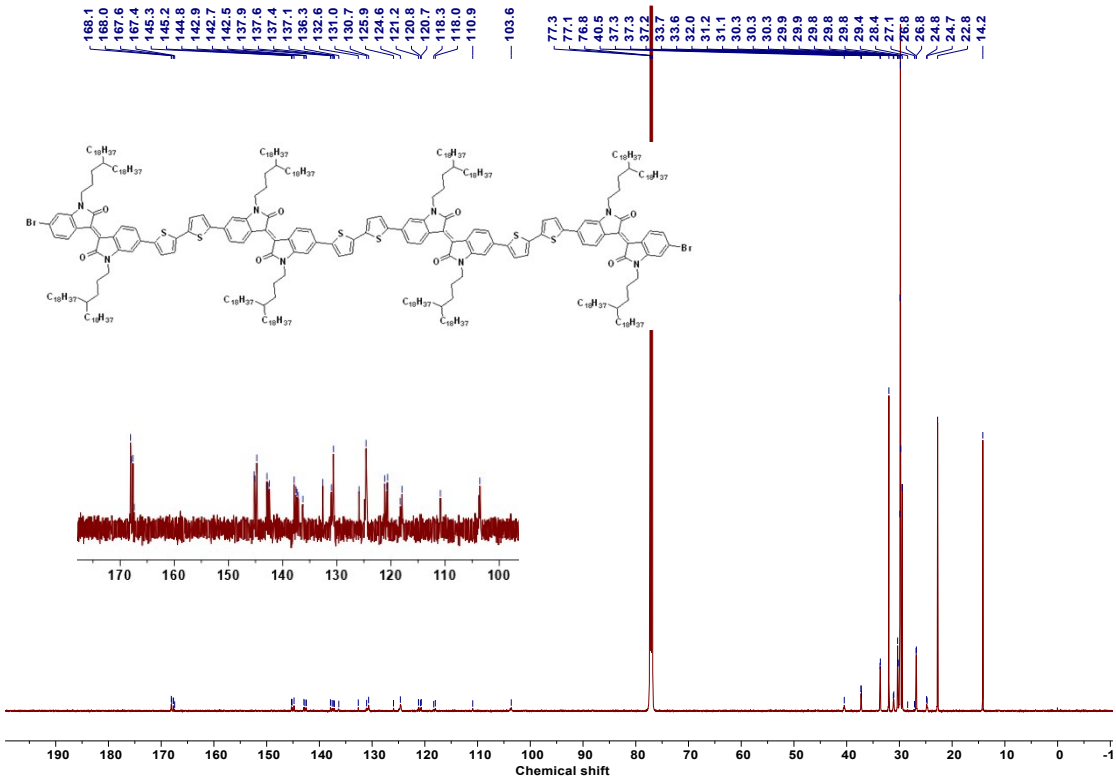

Figure S47. ^{13}C-NMR spectrum of 4IID-318 in $CDCl_3$ (151 MHz).

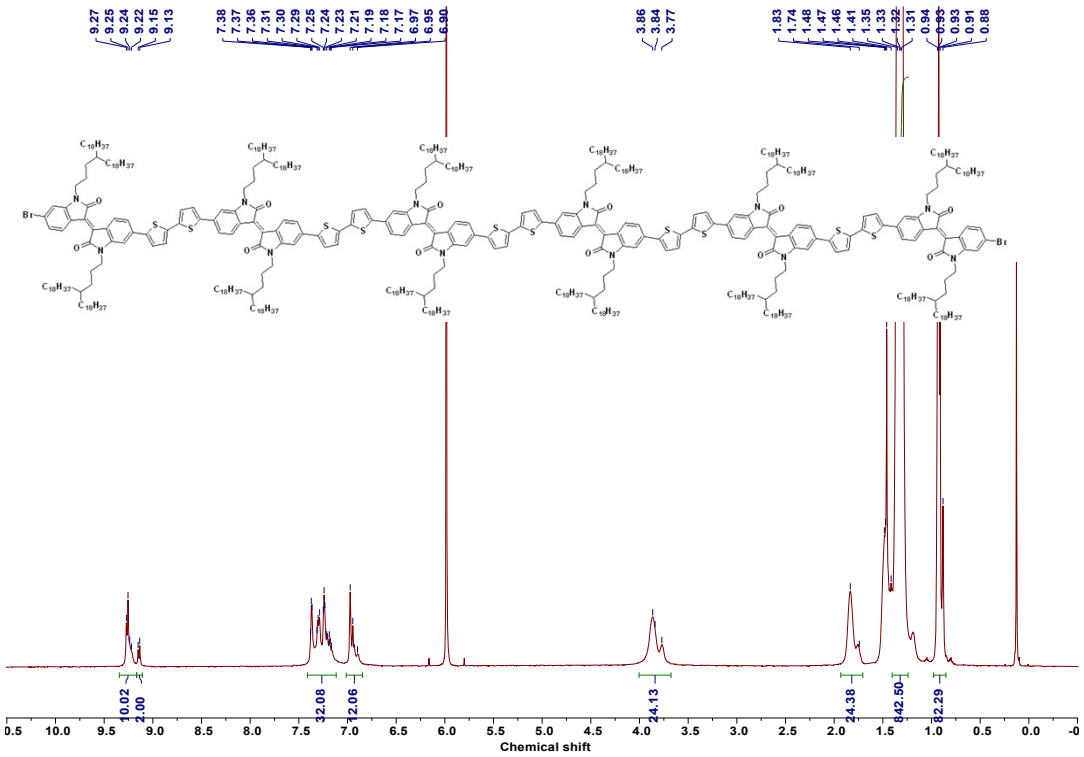

Figure S48. ^{1}H-NMR spectrum of 6IID-318 in $C_2D_2Cl_4$ (363 K, 500 MHz).

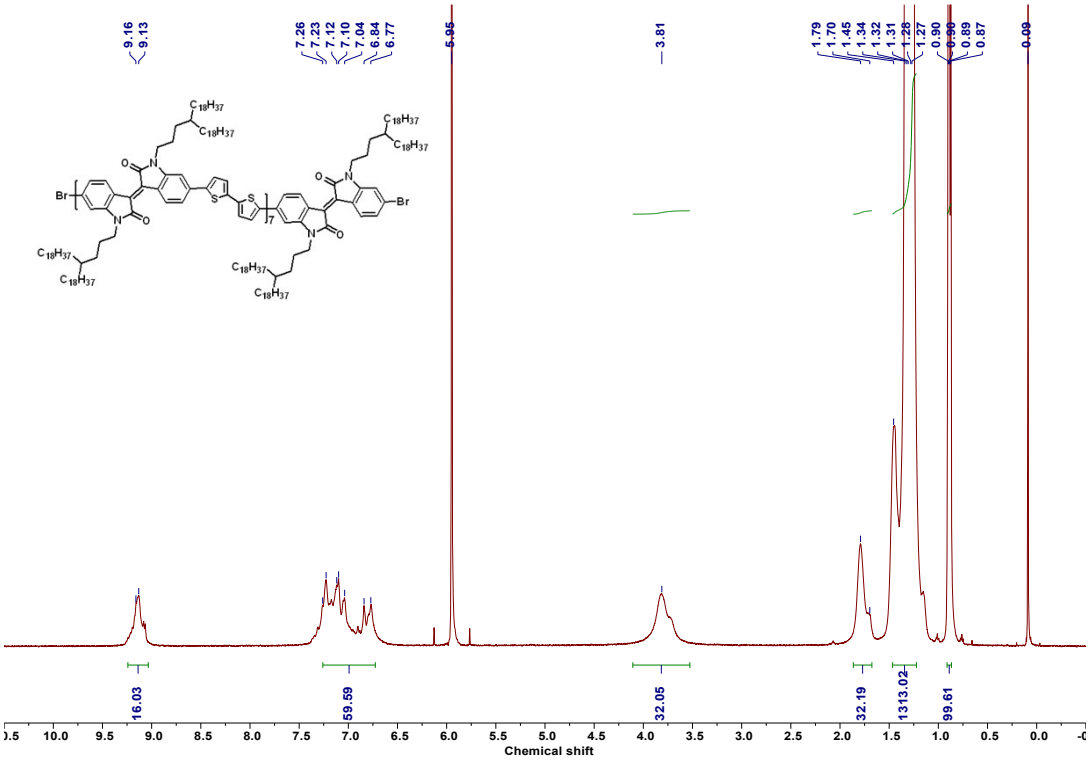

Figure S49. ^{1}H-NMR spectrum of 8IID-318 in $C_2D_2Cl_4$ (363 K, 500 MHz).

Reference:

1. T. Schuettfort, L. Thomsen, C. R. McNeill, *J. Am. Chem. Soc.,* 2013, **135,** 1092-1101.
2. M. Frisch, G. Trucks, H. Schlegel, G. Scuseria, M. Robb, J. Cheeseman, G. Scalmani, V. Barone, B. Mennucci, G. Petersson, 2009.
3. W. J. Hehre, R. Ditchfield, J. A. Pople, *J. Chem. Phys.,* 1972, **56,** 2257-2261.
4. R. L. C. Akkermans, N. A. Spenley, S. H. Robertson, *Mol. Simulat.,* 2021, **47,** 540-551.
5. Z.-F. Yao, Q.-Y. Li, H.-T. Wu, Y.-F. Ding, Z.-Y. Wang, Y. Lu, J.-Y. Wang, J. Pei, *SmartMat,* 2021, **2,** 378-387.
6. D. Venkateshvaran, M. Nikolka, A. Sadhanala, V. Lemaur, M. Zelazny, M. Kepa, M. Hurhangee, A. J. Kronemeijer, V. Pecunia, I. Nasrallah, I. Romanov, K. Broch, I. McCulloch, D. Emin, Y. Olivier, J. Cornil, D. Beljonne, H. Sirringhaus, *Nature,* 2014, **515,** 384-388.
7. D. W. Breiby, O. Bunk, J. W. Andreasen, H. T. Lemke, M. M. Nielsen, *J. Appl. Crystallogr.,* 2008, **41,** 262-271.
8. Y.-Y. Zhou, Y.-C. Xu, Z.-F. Yao, J.-Y. Li, C.-K. Pan, Y. Lu, C.-Y. Yang, L. Ding, B.-F. Xiao, X.-Y. Wang, Y. Shao, W.-B. Zhang, J.-Y. Wang, H. Wang, J. Pei, *Nat. Commun.,* 2023, **14,** 3340.
9. Y.-Y. Zhou, Z.-Y. Wang, Z.-F. Yao, Z.-D. Yu, Y. Lu, X.-Y. Wang, Y. Liu, Q.-Y. Li, L. Zou, J.-Y. Wang, J. Pei, *CCS Chem.,* 2021, **3,** 2994-3004.